Influence of Irradiation and Hydrolysis on Mechanical Properties and Crystallization in Selected Copolymers

Ing. Anna Švarcová, Ph.D.

Doctoral Thesis Summary

Tomas Bata University in Zlín

Tomas Bata University in Zlín
Faculty of Technology

Doctoral Thesis Summary

Influence of Irradiation and Hydrolysis on Mechanical Properties and Crystallization in Selected Copolymers

Vliv ozařování a hydrolýzy na mechanické vlastnosti a krystalizaci u vybraných kopolymerů

Author:	Ing. Anna Švarcová, Ph.D.
Degree programme:	P0531D130057 Technology of Macromolecular Substances
Degree course:	TML-0/ Technology of Macromolecular Substances
Supervisor:	prof. Ing. Petr Svoboda, Ph.D.
External examiners:	prof. Ing. Petr Slobodian, Ph.D. doc. Ing. Antonín Kuta, CSc.

Zlín, December 2025

Published by **Tomas Bata University in Zlín** in the Edition **Doctoral Thesis Summary.**
The publication was issued in the year 2025

Klíčová slova: *etylen-vinylacetát (EVA), ozařování elektronovým paprskem, zesíťování, mechanické vlastnosti při vysokých teplotách, krystalinita, kríp, napětí–deformace, frekvenční závislost, obsah gelu, biologicky rozložitelný polyester, poly(butylen-sukcinát-ko-adipát) (PBSA), hydrolýza, neizotermní krystalizace, izotermní krystalizace, distribuce molární hmotnosti, kinetika krystalizace, morfologie, polarizační optická mikroskopie (POM), sférolity, degradace, širokoúhlá rentgenová difrakce (WAXD)*

Keywords: *ethylene-vinyl acetate (EVA), electron beam irradiation, cross-linking, high-temperature mechanical properties, crystallinity, creep, stress–strain, frequency sweep, gel content, biodegradable polyester, poly(butylene succinate-co-adipate) (PBSA), hydrolysis, non-isothermal crystallization, isothermal crystallization, molecular weight distribution, crystallization kinetics, morphology, polarized optical microscopy (POM), spherulites, degradation, wide angle X-ray diffraction (WAXD)*

Full text of the doctoral thesis is available in the Library of TBU in Zlín.

ISBN 978-80-7678-388-1

I would like to express my sincere gratitude to my supervisor, prof. Ing. Petr Svoboda, Ph.D., for all the consultations, invaluable advice, and for dedicating the most precious resource we have - his time. I am especially grateful for his patience with me as a part-time student.

I would also like to thank God, as my faith has guided me to this point. My deepest thanks go to my family for their unwavering support since I began my studies at UTB in 2015.

Finally, I extend my gratitude to the army, which taught me how to fight and persevere.

ABSTRACT

The first part of the thesis investigates the effects of electron beam irradiation on polymeric structures. Particular attention is given to the influence of varying irradiation dose on cross-linking efficiency, crystallinity (X), and mechanical behavior. Experimental results demonstrate how irradiation modifies the material's resistance to deformation and enhances its thermal stability at elevated temperatures. The relationship between copolymer composition and the efficiency of cross-linking reactions is explored in detail, providing insights into the optimization of material performance through structural control.

The second part focuses on the hydrolytic degradation of the biodegradable copolyester poly(butylene succinate-co-adipate) (PBSA) under controlled laboratory conditions. The study evaluates the impact of hydrolysis on molecular weight, molecular weight distribution (MWD), and thermal properties such as melting (T_m) and glass transition temperatures $\left(T_g\right)$. Emphasis is placed on the changes in crystallization behavior and morphological evolution of the polymer, as observed at the microscopic level. These findings contribute to a deeper understanding of the long-term stability and environmental degradability of polymeric materials in various conditions.

This doctoral thesis summary presents a comprehensive and integrated analysis of the effects of electron beam irradiation and hydrolytic degradation on the physicochemical and mechanical properties of polymeric materials. The results contribute fundamentally to the design of advanced polymers with tunable performance parameters and provide a scientific basis for predicting their durability and functional behavior under demanding service conditions.

ABSTRAKT

První část práce zkoumá účinky ionizujícího záření na polymerní struktury. Je detailně popsán vliv různého stupně ozařování na zesíťovaní, krystalinitu (X) a mechanické chování. Měření prokazují, jak ozařování ovlivňuje odolnost materiálu vůči deformaci a jeho vysokoteplotní stabilitu. Pozornost je věnována vztahu mezi chemickým složením kopolymeru a účinností síťovacích reakcí, což poskytuje náhled na optimalizaci materiálových vlastností.

Druhá část se soustředí na hydrolytickou degradaci kopolyesteru poly(butylen-sukcinát-ko-adipátu) PBSA, simulovanou v kontrolovaných laboratorních podmínkách. Práce analyzuje, jak hydrolýza ovlivňuje molární hmotnost, její distribuci (MWD) a tepelné vlastnosti, jako jsou teploty tání (T_m) a skelného přechodu (T_g). Důraz je kladen na změny v krystalizačním chování a morfologii polymeru, které jsou pozorovány na mikroskopické úrovni. Tyto poznatky přispívají k pochopení dlouhodobé stability a rozložitelnosti polymerních materiálů v různých prostředích.

Celkově tyto teze poskytují komplexní a integrovaný pohled na to, jak ozařování a hydrolýza mění fyzikálně-chemické a mechanické charakteristiky polymerů. Získané poznatky jsou zásadní pro vývoj nových materiálů s řízenými vlastnostmi a pro predikci jejich životnosti a chování v náročných aplikačních podmínkách.

TABLE OF CONTENTS

1. INTRODUCTION

Polymer science plays a crucial role in the development of modern materials for applications ranging from medical devices and packaging to electronics and structural components. One of the most versatile strategies to tailor the performance of polymeric materials is through post-synthetic modification. This may be accomplished via physical means such as irradiation or by chemical and environmental degradation mechanisms like hydrolysis. Understanding the fundamental principles of these modifications and their influence on polymer structure is essential for predicting material behavior in both functional and end-of-life scenarios.

The rising demand for sustainable, recyclable, and high-performance materials has further increased interest in post-modification techniques. Polymer engineers and materials scientists are now focusing on optimizing the interplay between structure and function by combining empirical methods with theoretical modeling. This synergy is particularly crucial for designing materials with predictable service life and degradability, especially in light of increasing environmental regulations.

Among the various techniques, electron beam (EB) irradiation stands out as a controllable method to induce cross-linking in polymers, thereby improving their mechanical and thermal performance. It is an environmentally friendly and solvent-free technique that does not require chemical additives. On the other hand, hydrolytic degradation is a key mechanism for controlling the degradation profile of biodegradable polymers, especially polyesters. Polyesters are widely used in applications such as packaging, agriculture, and biomedicine, where controlled degradation is a desired feature.

This summary provides a theoretical overview of both modification strategies and the corresponding analytical approaches for evaluating polymer transformations, focusing on two representative copolymers: ethylene-vinyl acetate (EVA) and poly(butylene succinate-co-adipate) (PBSA). EVA is known for its flexibility, transparency, and compatibility with irradiation techniques, while PBSA is a prominent biodegradable polyester with promising thermal and mechanical properties.

AIM OF THE DOCTORAL THESIS

The aim of the doctoral thesis is to investigate the influence of two modification pathways – electron beam irradiation and hydrolysis – on the physicochemical and mechanical properties of selected copolymers. Specifically, the thesis intends to:

- Evaluating the effects of EB irradiation on crystallinity, cross-linking efficiency, and viscoelastic behavior of EVA copolymers.
- Assessing the impact of hydrolytic degradation on molecular weight distribution, crystallization kinetics, and morphology of PBSA.
- Summarize the key analytical models and methods used to characterize polymer changes.

The overarching goal is to provide a comprehensive theoretical understanding of how these processes influence polymer structure and behavior.

2. THEORETICAL BACKGROUND

2.1.1 Effects of electron beam ionizing method of radiolysis of copolymer EVA

Electron beam irradiation is a physical modification technique that uses accelerated electrons to initiate chemical reactions within polymer matrices [1]. Compared to chemical cross-linking methods, EB cross-linking offers several advantages: it does not introduce residual chemicals, allows precise control of modification depth, and can be carried out at room temperature [2]. The primary outcomes of EB irradiation are chain scission and cross-linking, with the latter being the more desirable effect for enhancing polymer performance [3]. In cross-linking, radicals generated by high-energy electrons react to form covalent bonds between polymer chains, resulting in a three-dimensional network that limits molecular mobility [4].

The effectiveness of EB induced cross-linking depends on the chemical structure of the polymer, the absorbed dose (typically measured in kGy), the dose rate, and the presence of oxygen or other reactive species [5]. For ethylene-vinyl acetate (EVA), the vinyl acetate (VA) content plays a critical role [6]. Copolymers with higher VA content tend to produce more radicals upon irradiation, facilitating network formation [7]. However, too high a dose can lead to chain scission, thereby compromising mechanical properties [8].

Cross-linked EVA demonstrates increased thermal stability, improved creep resistance, and reduced shrinkage, making it suitable for applications in cable insulation [9-12], foams [7, 13, 14], and encapsulants [15, 16]. Models such as the four-parameter Burgers and six-parameter viscoelastic models are used to describe this behavior. Cross-link density can be quantified using dynamic mechanical analysis and interpreted via the Charlesby-Pinner and Charlesby-Rosiak equations that help to interpret gel content and sol fraction data, providing insight into the balance between cross-linking and degradation reactions.

Numerous studies [11, 17, 18] have examined the kinetics of radical formation, the role of crystallinity in radical recombination, and the long-term stability of irradiated EVA [6].

While electron beam cross-linking of EVA and its polymer blends has been addressed in the literature, most of these studies focus on general cross-linking behavior or thermal performance in blended systems. However, to the best of our knowledge, there is a lack of systematic investigation into how varying vinyl acetate (VA) content influences the high-temperature creep resistance of electron beam cross-linked neat EVA copolymers. This thesis aims to address this specific gap by linking EVA composition to post-irradiation structural and viscoelastic performance under elevated temperature conditions.

2.1.2 Cross-linking vs. chain scission

Electron beam irradiation of ethylene-vinyl acetate (EVA) copolymers leads to significant structural modifications through the competing processes of cross-linking and chain scission. These reactions directly affect the molecular weight distribution and chain architecture, with profound implications for the material's viscoelastic behavior. In its unmodified, semicrystalline state, EVA contains long polymer chains that contribute to physical entanglements. These entanglements act as temporary cross-links that restrict chain mobility and improve creep resistance, particularly at moderate temperatures [19].

In addition to entanglements, long-chain segments in the amorphous phase function as tie molecules, which span between crystalline lamellae and facilitate stress transfer under mechanical load. The presence and integrity of these tie molecules are crucial for maintaining dimensional stability under sustained stress.

Upon exposure to electron beam radiation, chain scission events can reduce the average molecular weight of EVA, leading to a decrease in chain entanglements and a lower population of tie molecules. This structural degradation weakens the interlamellar cohesion and increases the mobility of shorter molecular fragments, thereby compromising the polymer's resistance to creep deformation. As a result, creep compliance increases, particularly at lower irradiation doses or when scission predominates over cross-linking.

Although chain scission may occur during irradiation, the cross-linked EVA structure formed at relatively low irradiation temperatures (below 50 °C) significantly enhances creep resistance when the material is subjected to high operating temperatures such as 150 °C. At these elevated temperatures, the effect of covalent network formation becomes dominant, as the permanent cross-links restrict chain mobility far more effectively than physical entanglements alone. This results in a noticeable reduction in creep compliance despite the potential decrease in molecular weight due to scission.

The proposed mechanism of electron beam induced cross-linking in EVA is illustrated in Figure 1.

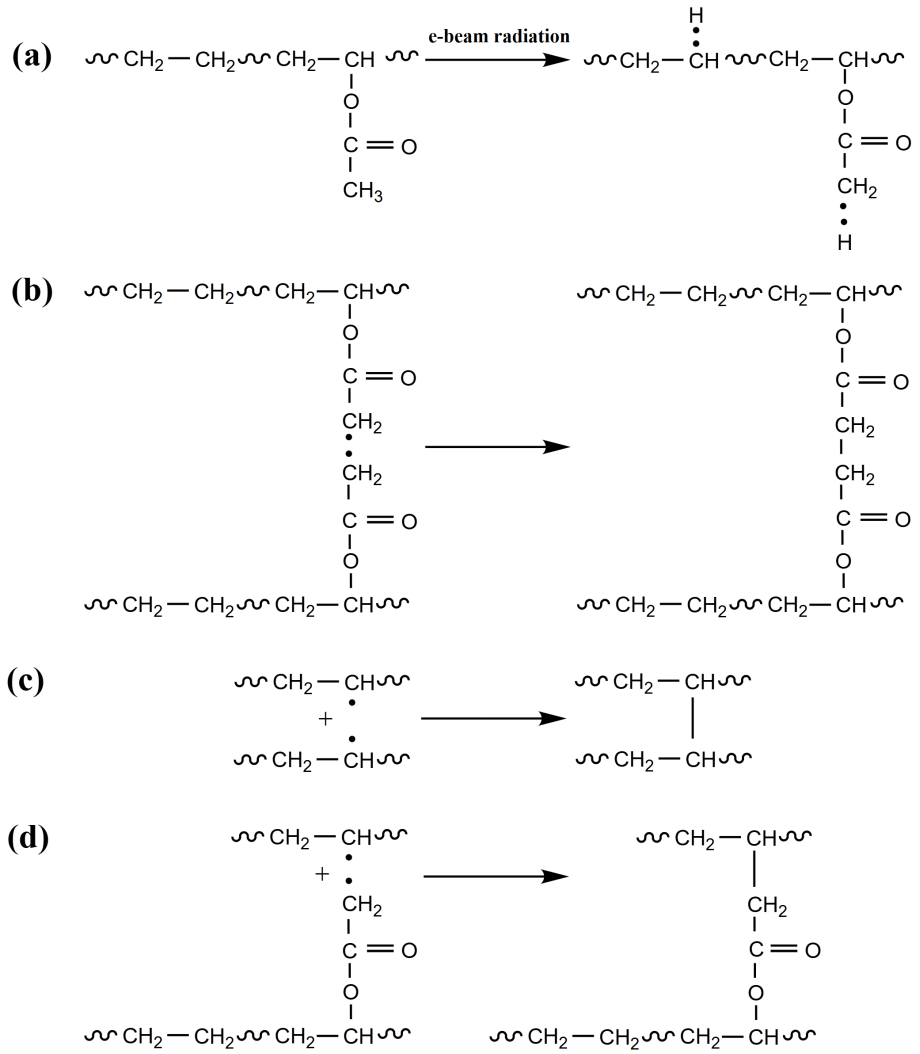

Figure 1. Possible cross-linking mechanism—chemistry: (a) generation of free radicals by irradiation; (b) cross-linking between vinyl acetate branches; (c) cross-linking between ethylene units; and (d) cross-linking between vinyl acetate branch and ethylene unit.

2.2 Hydrolysis of PBSA

Hydrolysis of aliphatic polyesters is a complex process governed by chemical kinetics, diffusion, and morphological factors [20-24]. In the case of PBSA, a random copolyester composed of butylene succinate (BS) and butylene adipate (BA) units, hydrolysis primarily occurs through bulk degradation. Water penetrates the polymer matrix and cleaves ester bonds, resulting in a reduction of molar mass and an increase in chain end concentration [25, 26].

The rate of hydrolysis is influenced by the degree of crystallinity, since amorphous domains are more permeable to water and thus more susceptible to hydrolytic attack [27]. In contrast, crystalline domains act as physical barriers. As degradation proceeds, crystalline lamellae may reorganize or grow due to secondary crystallization, leading to changes in the thermal and mechanical properties [28].

Environmental factors such as temperature, pH, and enzymatic activity further modulate the hydrolysis pathway. At elevated temperatures, such as 50–70 °C, hydrolysis accelerates significantly, making it a valuable model for predicting long-term degradation under composting or physiological conditions. Additionally, the chemical composition of PBSA enables tunability of degradation rate by adjusting the BA:BS ratio [21].

In the case of PBSA, the hydrolysis process has been interpreted using a combination of kinetic models, dependence on the crystallinity, sample geometry, and degradation stage. Experimental data often show a combination of these effects, dependence on sample thickness, crystallinity, and degradation time. Crystallization kinetics before and after hydrolysis are typically analyzed using models such as Avrami, Ozawa, and Hoffman–Lauritzen. These models provide insight into nucleation mechanisms, crystal growth rates, and lamellar thickness evolution. Thermodynamic interpretations are further supported by the Gibbs–Thomson equation, which relates melting temperature to crystal size.

These analytical approaches allow for a comprehensive understanding of the hydrolysis-induced structural changes and offer predictive capability for polymer design in biodegradable applications.

2.2.1 Isothermal and non-isothermal crystallization

Crystallization significantly affects the morphology, thermal behavior, and mechanical performance of semicrystalline polymers. In polymer science, two primary thermal regimes are used to investigate crystallization kinetics: isothermal and non-isothermal. Each provides different insight into the nucleation and growth mechanisms of crystalline structures and is selected based on the objective of the study.

Isothermal crystallization occurs when the polymer is held at a constant temperature, enabling detailed time-resolved analysis of spherulitic growth. This approach allows researchers to apply kinetic models such as the Avrami equation, which reveals the dimensionality of crystal growth and the nature of nucleation processes. The controlled temperature environment makes it easier to isolate variables and interpret the intrinsic crystallization behavior of the polymer.

Non-isothermal crystallization, on the other hand, occurs during a continuous change in temperature typically cooling from the melt. This method simulates real-world industrial processing conditions such as injection molding and extrusion. It provides more realistic data on crystallization onset, peak temperature, and crystallization rate under dynamic thermal conditions. Models such as the Ozawa, Jeziorny (modified Avrami) equations are often used to describe non-isothermal kinetics and derive activation energy values.

Recent review papers have provided comprehensive guidance on the application of these models. A 2023 review in Processes outlines the theoretical basis and practical limitations of the application of Avrami, Arrhenius, and isoconversional models to non-isothermal DSC data, especially in semi-

crystalline systems undergoing thermal or chemical modification. The review emphasizes the importance of model selection and highlights scenarios where isoconversional analysis yields more reliable results than classical single-value approaches [29].

Experimental work on various copolymers, including poly(ethylene chlorotrifluoroethylene) (ECTFE) and polyvinylidene fluoride PVDF, has demonstrated the usefulness of both thermal regimes for study of morphology development. Yang et al. applied isothermal and non-isothermal DSC and POM to ECTFE, using Avrami and Ozawa models to extract kinetic parameters and interpret nucleation behavior [30]. Pérez et al. studied PVDF polymorphs and confirmed the influence of cooling rate on polymorphic selection and crystal growth in non-isothermal settings [31].

In the context of biodegradable copolyesters such as PBSA, both crystallization regimes are particularly relevant. Non-isothermal experiments reveal how hydrolysis and thermal history influence crystallization onset, morphology, and nucleation density, while isothermal measurements provide clearer insight into growth rates and lamellar reorganization. Together, they offer an analytical framework for understanding how morphological and thermal transitions influence the functional behavior of biodegradable polymers during degradation and processing.

EXPERIMENTAL PART

3. MATERIALS AND METHODS

Two polymeric systems were selected for this study, each representing a distinct approach to material modification. The first system was based on ethylene-vinyl acetate (EVA) copolymers differing in vinyl acetate (VA) content, selected to investigate how comonomer concentration influences the cross-linking efficiency and high-temperature behavior after electron beam irradiation. The second system involved a biodegradable aliphatic polyester, poly(butylene succinate-co-adipate) (PBSA), chosen for its sensitivity to hydrolysis and its relevance in environmentally degradable applications. All materials were used in granulate form and processed under controlled conditions to ensure consistency in sample preparation.

The EVA materials, denoted EVA 206 and EVA 212, contained 6 wt.% and 12 wt.% VA respectively, and were subjected to irradiation under ambient atmosphere. The PBSA samples, on the other hand, were exposed to controlled hydrolytic conditions at elevated temperatures (37-70 °C) to monitor changes in crystallization behavior and molecular weight over time.

The accurate characterization of structural and property changes in polymers requires a combination of complementary analytical techniques (see Appendix A-B). Each method contributes to a specific aspect of polymer behavior, from thermal transitions and molecular architecture to morphological features and dynamic mechanical properties. Below is a detailed overview of the techniques commonly used in studies involving electron beam irradiation and hydrolytic degradation.

3.1 Ethylene-vinyl acetate (EVA)

EVA is a random copolymer of ethylene and vinyl acetate (VA), classified as a semi-crystalline polyolefin. It is synthesized through free-radical polymerization of ethylene and vinyl acetate monomers, typically under high pressure. The properties of EVA depend strongly on the VA content, which typically ranges between 1-40 wt.%. As the VA content increases, the material becomes more flexible, less crystalline, and more polar. This comonomer effect also influences the polymer's response to irradiation, as VA units stabilize radicals and promote cross-linking.

In this work, two EVA copolymers were used: EVA 206 with 6 wt.% VA and EVA 212 with 12 wt.% VA (see Figure 2). These were selected to evaluate how increasing VA concentration affects radiation-induced network formation and mechanical performance at elevated temperatures.

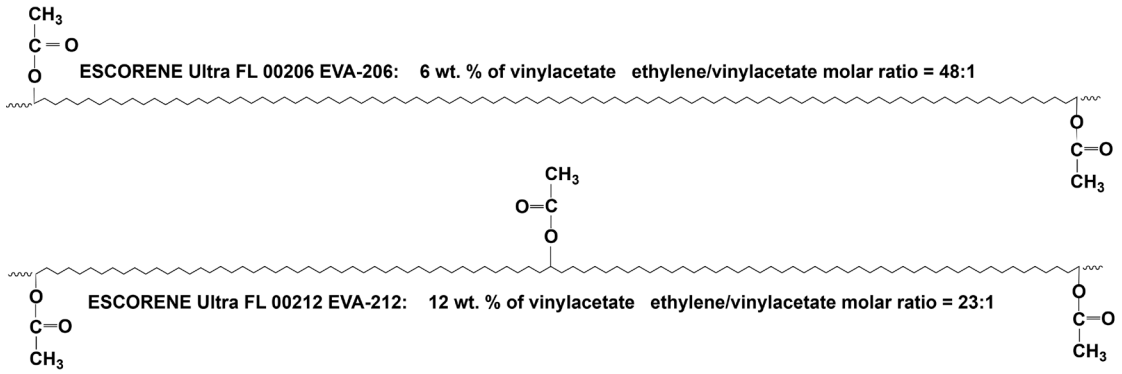

Figure 2. Chemical structure of EVA copolymers.

The fundamental properties of the EVA materials employed in this study are summarized in Table 1

Table 1. Composition and density of investigated ethylene vinyl acetate copolymers (EVA)

Material	**VA**	**Ethylene**	**VA**	**Ethylene**	**Density**	**ET/VA (molar ratio)**
Abbreviation	wt. %	wt. %	mol %	mol %	g/cm^3	-
EVA-206	6	94	2.04	97.96	0.926	48.1
EVA-212	12	88	4.26	95.75	0.934	22.5

MFI at 190°C was for both samples 2.0 g/10 min

3.2 PBSA

PBSA is a biodegradable aliphatic copolyester composed of butylene succinate and butylene adipate units. It is synthesized via polycondensation of succinic acid (or its dimethyl ester), adipic acid, and 1,4-butanediol (see Figure 3). Due to its biodegradability, flexibility, and moderate crystallinity, PBSA is widely used in compostable packaging, agricultural films, and biodegradable fibers.

The presence of flexible adipate units lowers the melting temperature and crystallinity compared to poly(butylene succinate) (PBS), making PBSA more suitable for applications requiring faster degradation. In this study, PBSA was subjected to controlled hydrolytic degradation to investigate how molecular weight, crystallization behavior, and morphology evolve during environmental exposure.

Tables 2 and 3 summarize the fundamental properties of PBSA, including its density and thermal parameters such as heat distortion temperature (HDT).

All reagents used for hydrolysis experiments in phosphate-buffered saline were supplied by Merck KGaA, Darmstadt, Germany.

Table 2. Material properties and bulk density of the analyzed poly(butylene succinate-co-butylene adipate) PBSA.

Material	**Molecular weight**	**Elongation at break**	**Tensile strength**	**Young's modulus**	**Density**
Abbreviation	g/mol	(%)	(MPa)	(MPa)	g/cm^3
PBSA	1.08×10^5	780	40	320	1.23

MFI was 3.0 g/10 min

Table 3. Thermal properties of investigated PBSA copolymer.

Material	**Melting point**	**Glass transition temperature**	**Heat of combustion (kJ/g)**	**HDT at 0.45 MPa**
Abbreviation	(°C)	(°C)	(kJ/g)	(°C)
PBSA	94	-45	23.9	69

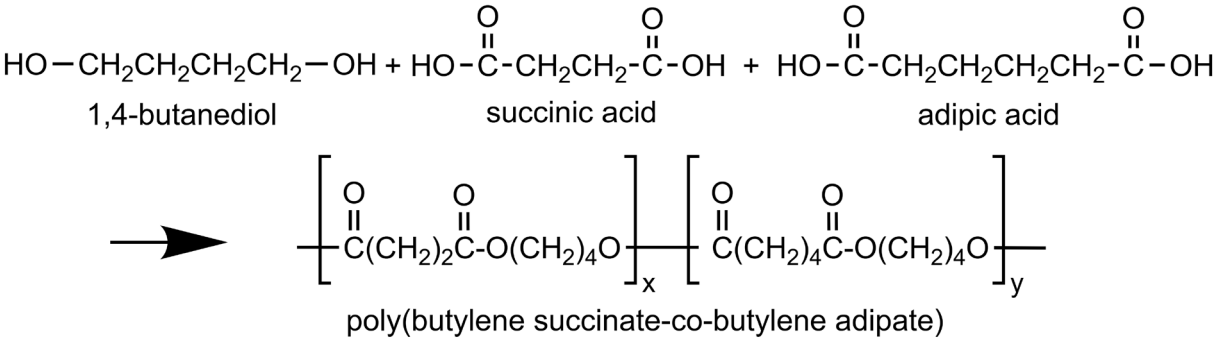

Figure 3. Chemical structure of 1,4-butanediol, succinic acid, adipic acid, and poly(butylene succinate-co-butylene adipate)

3.3 Dynamic mechanical analysis (DMA)

DMA measures the viscoelastic response of polymers under oscillatory stress as a function of temperature, time, or frequency. It provides valuable information about the storage modulus (G'), elastic response, loss modulus (G'') viscous response and damping behavior $(\tan\delta)$. These parameters are particularly useful in detecting transitions such as the glass transition temperature (T_g) and in evaluating cross-linking density and molecular mobility. In cross-linked systems, increased storage modulus and a more pronounced rubbery plateau often indicate a higher degree of network formation.

3.3.1 Dynamic mechanical analysis (DMA) of EVA

Dynamic mechanical performance was evaluated using a DMA-1 STARe System (Mettler-Toledo GmbH, Greifensee, Switzerland). Three types of measurements were conducted to assess creep behavior, frequency dependence, and stress–strain response. The tests were performed in shear mode on rectangular specimens (11 × 11 × 1 mm) at two temperatures: 25 °C and 150 °C. Experimental conditions for each test are summarized in Tables 4–6. The testing setup is illustrated in Figures 4 and 5. For each condition, three individual measurements were performed and their average value was reported.

Table 4 DMA creep testing conditions

Test	**Mode**	**Force (N) at time (0-1 min)**	**Force (N) at creep (1-5 min)**	**Force (N) at recovery (5-10 min)**
creep	static	0.05	1	0.05

Table 5 DMA frequency sweep testing conditions

Test	**Displacement (µm)**	**Frequency (Hz)**	**Force (N)**
Frequency sweep	10	0.1-100	0.1

Table 6 DMA stress-strain testing conditions

Test	**Force (N)**	**Force rate (N/min)**	**Shear strain (%) for shear stress evaluation**
Stress-strain	0-2	0.4	0.03

Tests were carried out at 25 °C and 150 °C using shear deformation.

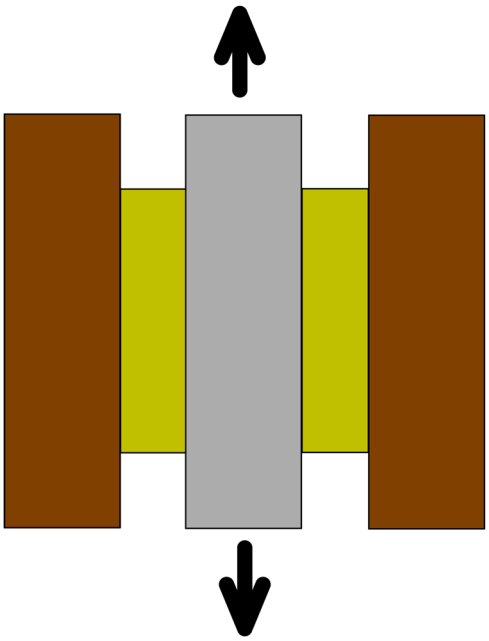

Figure 4. Shear mode of testing in Dynamic Mechanical Analyzer. Brown rectangles represent static metal pieces, yellow-green rectangles represent measured samples (two pieces) and grey rectangle is the central moving part where black arrows show direction of movement. The movement of the central part (grey rectangle) is recorded. Many parameters were evaluated such as $G', \eta^*, \tan\delta$ *as a function of frequency in range 0.1-100 Hz.*

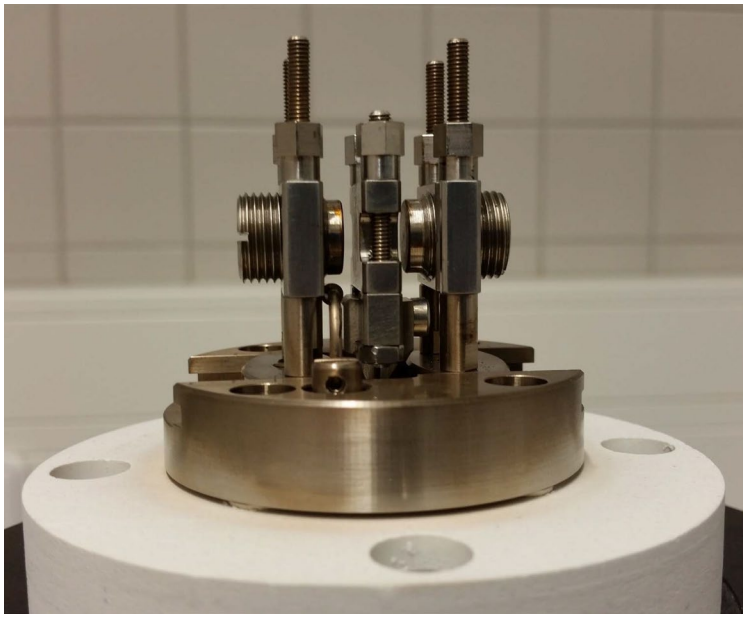

Figure 5. Shear testing fixture of Dynamic Mechanical Analyzer.

3.4 Gel content and cross-linking determination

3.4.1 Gel content in cross-linked EVA

To determine the gel content of electron beam cross-linked EVA 206 and EVA 212 samples, solvent extraction was performed according to ASTM D2765-01 [32]. The insoluble fraction remaining after refluxing in xylene was used to calculate the gel content as a percentage of the sample's final weight (m_1) to its initial weight (m_0). The final value represents the average of three measurements.

The gel content was calculated using the following formula [33].:

$$\text{gel content (\%)} = \frac{m_1}{m_0} \times 100 \quad (1)$$

Figure 6 illustrates the evolution of gel content in EVA 206 and EVA 212 as a function of dose. A steep increase in gel fraction was observed between 60 and 120 kGy, followed by a more gradual rise up to 180 kGy. EVA 212 consistently exhibited higher gel content compared to EVA 206, indicating more efficient cross-linking, likely due to its higher vinyl acetate content. These findings are consistent with previous studies by Wang et al. [34], Datta et al. [35], and Ali and Legocka [36], who also reported a dose dependent increase in gel content in polyolefin systems subjected to electron beam irradiation.

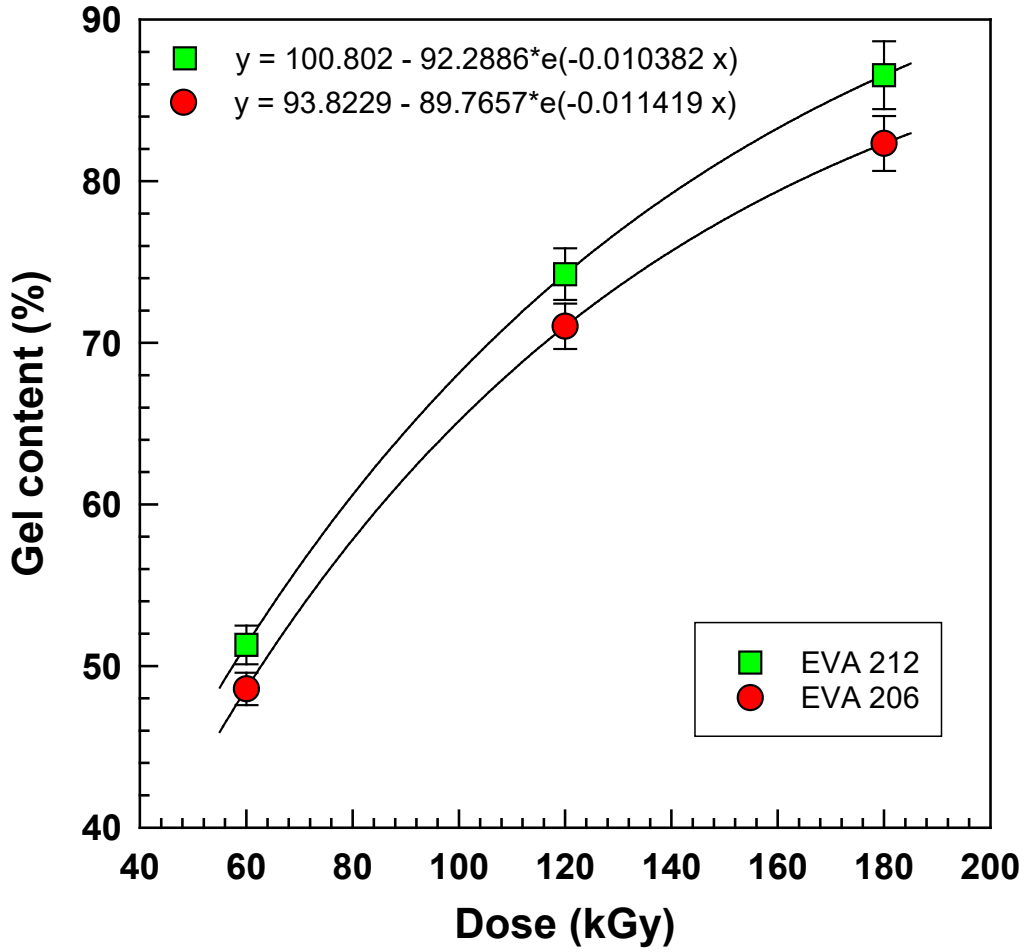

Figure 6. Gel content vs. dose for two radiation cross-linked ethylene-vinyl acetate copolymers.

The gel fraction increases with rising irradiation dose, as more covalent bonds are introduced into the polymer structure, leading to network formation. However, beyond a certain dose, competing chain scission may reduce gel yield or alter network homogeneity. To better understand the balance between cross-linking and degradation processes, analytical models such as the Charlesby–Pinner and Charlesby–Rosiak equations are employed. These models relate the sol fraction and absorbed dose to estimate cross-linking (q_0) and scission (p_0) yields, providing insight into the prevailing reaction mechanism.

By combining experimental measurements with theoretical modeling, it is possible to comprehensively assess the efficiency of electron beam induced cross-linking in EVA copolymers and to compare structural differences related to vinyl acetate content.

3.4.2 Charlesby–Pinner equation

Cross-linking efficiency in irradiated polymers is frequently evaluated using the Charlesby–Pinner equation [37], which establishes a relationship between the sol fraction (s), the radiation dose (D), and the yields expressed using G values, specifically of chain scission $(G_S), (p_0)$ and cross-linking $(G_x), (q_0)$.

This approach enables quantification of competing modification reactions during polymer irradiation.

The classical form of the equation is :

$$s + \sqrt{s} = \frac{p_0}{q_0} + \frac{1}{q_0 P_n D} \qquad (2)$$

where:

s is the soluble fraction (non-crosslinked portion);

$g = 1 - s$ is the gel fraction;

p_0 and q_0 denote sccision and cross-link probabilities per unit dose, respectively;

P_n is is the initial number-averaged degree of polymerization;

D is the absorbed dose in kGy.

In Figure 7 plotting $s + \sqrt{s}$ versus $1/D$ yields a linear relationship; the intercept gives p_0/q_0 and the slope allows calculation of q_0 and G values.

Such plots are regularly used in the literature to evaluate the cross-linking behavior in polyethylene, EVA, PVDF, and other polymers [38-41].

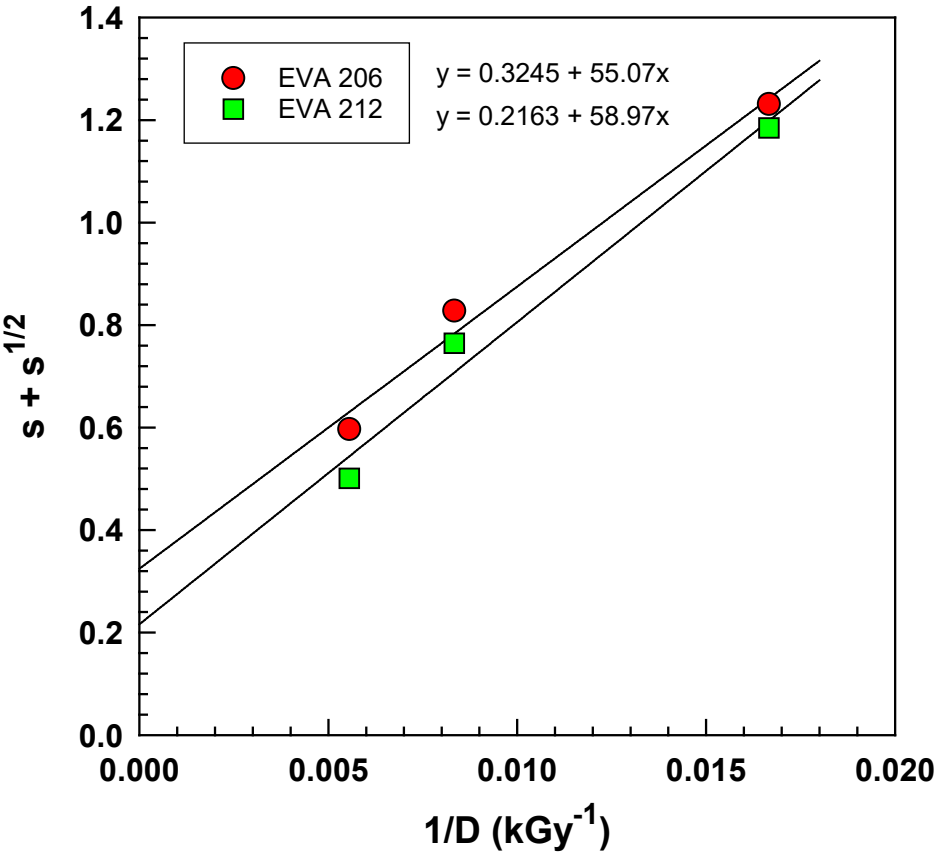

Figure 7. Quantitative Charlesby–Pinner analysis: $s + s^{1/2}$ vs. $1/D$ of EVA 206 and EVA 212 yielding slope and intercept values used for calculation shown in Appendix C.

3.4.3 Charlesby–Rosiak equations

The Charlesby–Rosiak model refines the original equation by adjusting for broader polydispersity and radical mobility effects, thus improving the fit when the initial molecular weight distribution deviates from the ideal. Olejniczak et al. [42] introduced an extended form of the Charlesby–Pinner model, which is now known as the Charlesby–Rosiak equation.

$$s + \sqrt{s} = \frac{p_0}{q_0} + \left(2 - \frac{p_0}{q_0}\right)\left(\frac{D_v + D_g}{D_v + D}\right) \qquad (3)$$

where:
D_V is the virtual dose;
D_g is the gelation dose

Figure 7 illustrates the analysis of sol fraction data plotted as $s + \sqrt{s}$ versus $1/D$ the reciprocal of the absorbed dose based on the Charlesby–Pinner equation. A deviation from ideal linearity was observed, likely due to the molecular weight distribution deviating from the assumed ratio $M_w/M_n = 2$. To account for this,

a modified version of the model known as the Charlesby–Rosiak equation was applied. The plot is shown in Figure 8. This approach improves accuracy when analyzing cross-linked polymers with broader polydispersity and has been widely adopted in literature for various polymer systems [42-46].

Using this refined model, cross-linking and scission parameters can be extracted more reliably. The radiation chemical yield ratio p_0/q_0, representing the balance between chain scission and cross-linking, was found to be lower for EVA 212 than for EVA 206, indicating a higher tendency toward cross-linking in the copolymer with increased vinyl acetate content.

Due to reduced chain scission in EVA 212, the ratio of cross-linking to degradation yield, $G(X)/G(S)$ was elevated. The calculation was performed using Equation 4.

$$\frac{G(X)}{G(S)} = \frac{1}{2\frac{p_0}{q_0}} \qquad (4)$$

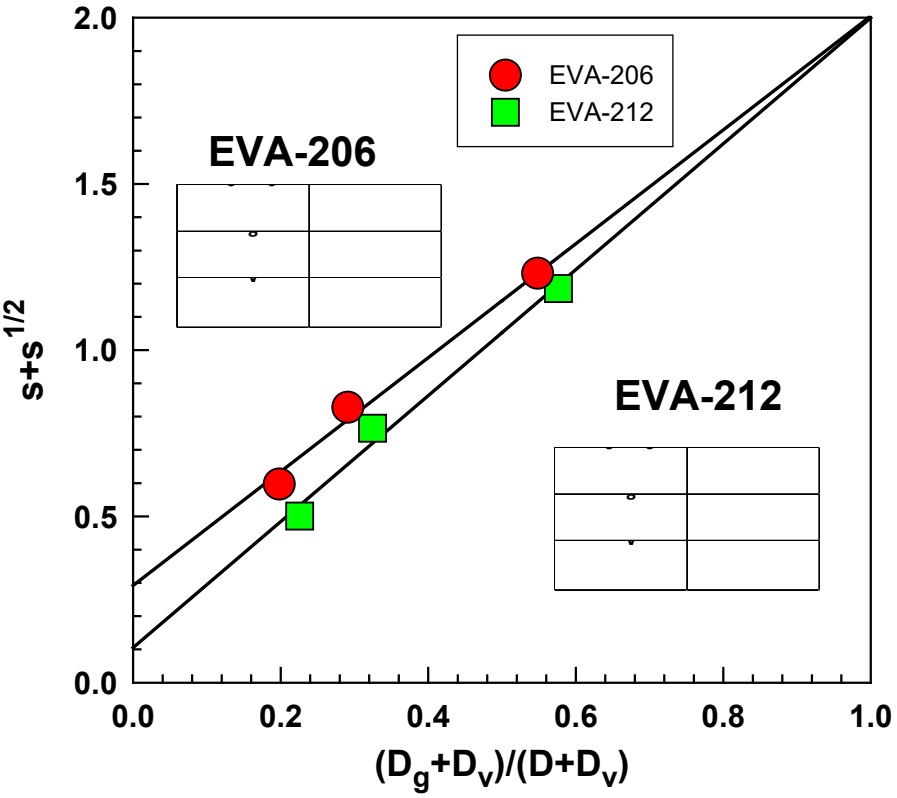

Figure 8. Experimental data of the sol-gel analysis for the EVA copolymers, shown in Charlesby-Rosiak coordinates.

In addition to sol-gel analysis, rheological methods offer an effective means to estimate cross-link density X by Equation 5, especially in lightly cross-linked systems where gel fraction measurements may lack sensitivity. Mussatti and Macosko [47], proposed using the complex modulus G^*or more specifically the storage modulus G', measured in the rubbery plateau region of a DMA test. The molecular weight between cross-links (M_C) can be estimated using Equation 6:

$$X = \frac{G^*}{R \cdot T} \qquad (5)$$

where,
G^* is complex modulus in Pa.
X is crosslinking density (mol/m³)
R is the gas constant 8.314 J K^{-1} mol^{-1}
T is the absolute temperature (in our case 423.15 K).

$$M_C = \frac{\rho RT}{G'} \qquad (6)$$

where,
ρ is the density of the amorphous polymer.

Furthermore, the Flory–Huggins theory provides a thermodynamic framework for analyzing polymer–solvent interactions and swelling behavior in cross-linked networks. When combined with equilibrium swelling experiments, it enables calculation of cross-link density based on network elasticity and polymer–solvent affinity parameters [48].

The cross-link density ν_d is then:

$$\nu_d = \frac{\rho}{M_C} = \frac{\rho}{\frac{\rho RT}{G'}} \qquad (7)$$

Figure 9(a) presents the complex shear modulus G^* which increases linearlly with the irradiation dose. Notably, higher values were recorded for EVA 212 across the studied dose range. Figure 9(b) illustrates the cross-link density X at a frequency of 0.1 Hz, calculated according to Equation 6. A consistent upward trend with increasing irradiation dose was observed, and the cross-link density values were again higher for EVA 212 compared to EVA 206.

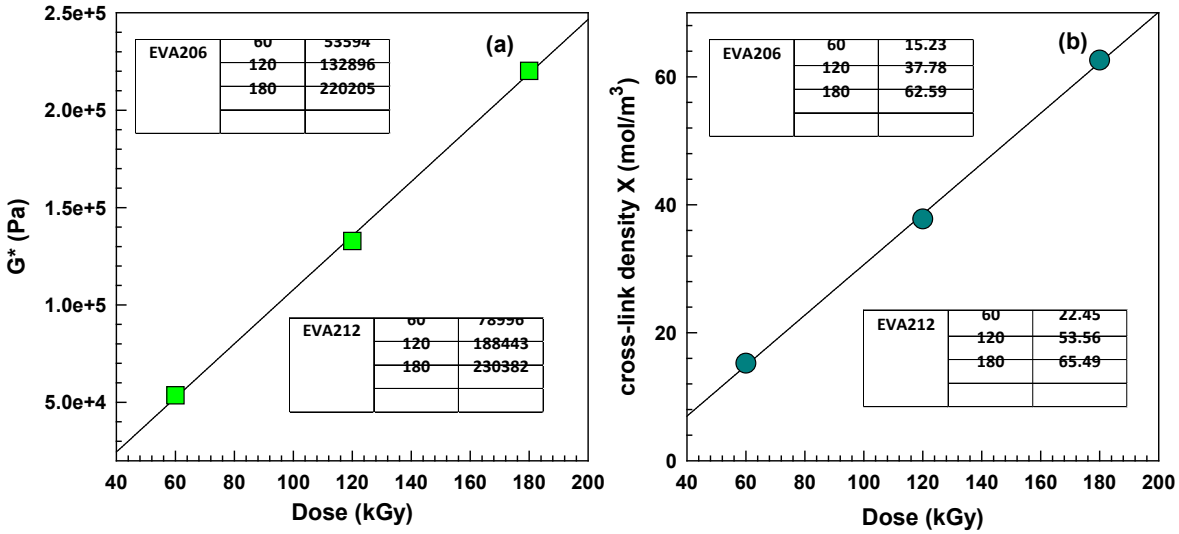

Figure 9. (a) Complex shear modulus G, (b) cross-link density X for copolymer EVA 206 and 212 at frequency of 0.1 Hz.*

3.5 Hydrolysis conditions and evaluation

Hydrolysis experiments were carried out using phosphate-buffered saline (PBS) solution. The buffer was prepared by dissolving 8 g of NaCl, 200 mg of KCl, 1.44 g of Na_2HPO_4, and 240 mg of KH_2PO_4 in 800 mL of distilled water. The pH was adjusted to 7.2, and the volume was brought up to 1 L with distilled water. To inhibit microbial growth, sodium azide (NaN_3) was added to the solution.

Polymer films of PBSA were cut into 5 × 5 mm pieces, and 200 mg portions were placed into 250 mL biometric flasks filled with 200 mL of PBS buffer. The flasks were placed in a Memmert UFE 400 oven set to 37 °C, 58 °C, or 70 °C, with ±1 °C stability. The contents were continuously stirred throughout the test. Samples were withdrawn at 4, 8, 16, 32, and 64 days to monitor hydrolytic degradation.

Two approaches were used to evaluate the degree of hydrolysis. First, mass loss of the solid polymer after drying and weighing was used to determine hydrolysis progress. Second, dissolved organic carbon (DOC) was measured in the buffer using a Shimadzu TOC 5000A analyzer. For each time point, triplicate 50 µL aliquots were analyzed, and results were expressed in mg/L.

Figure 10 illustrates the degree of hydrolysis of PBSA as a function of time at 37 °C, 58 °C, and 70 °C. The extent of hydrolysis increased significantly with temperature. After 64 days, the hydrolysis levels were 6.5 %, 31.7 %, and 49.5 % for 37, 58, and 70 °C, respectively. Analysis of the slope between days 16 and 64 revealed values of 0.0671, 0.4351, and 0.6556, further confirming accelerated hydrolysis at elevated temperatures. These findings are consistent with those of Wang et al. [49] in 2020, who reported enhanced degradation of PLA-based materials at higher temperatures. Wang et al. [50] in 2022 also observed higher hydrolysis rates in glycolic acid copolymers compared to virgin PLA, under both aquatic and soil conditions.

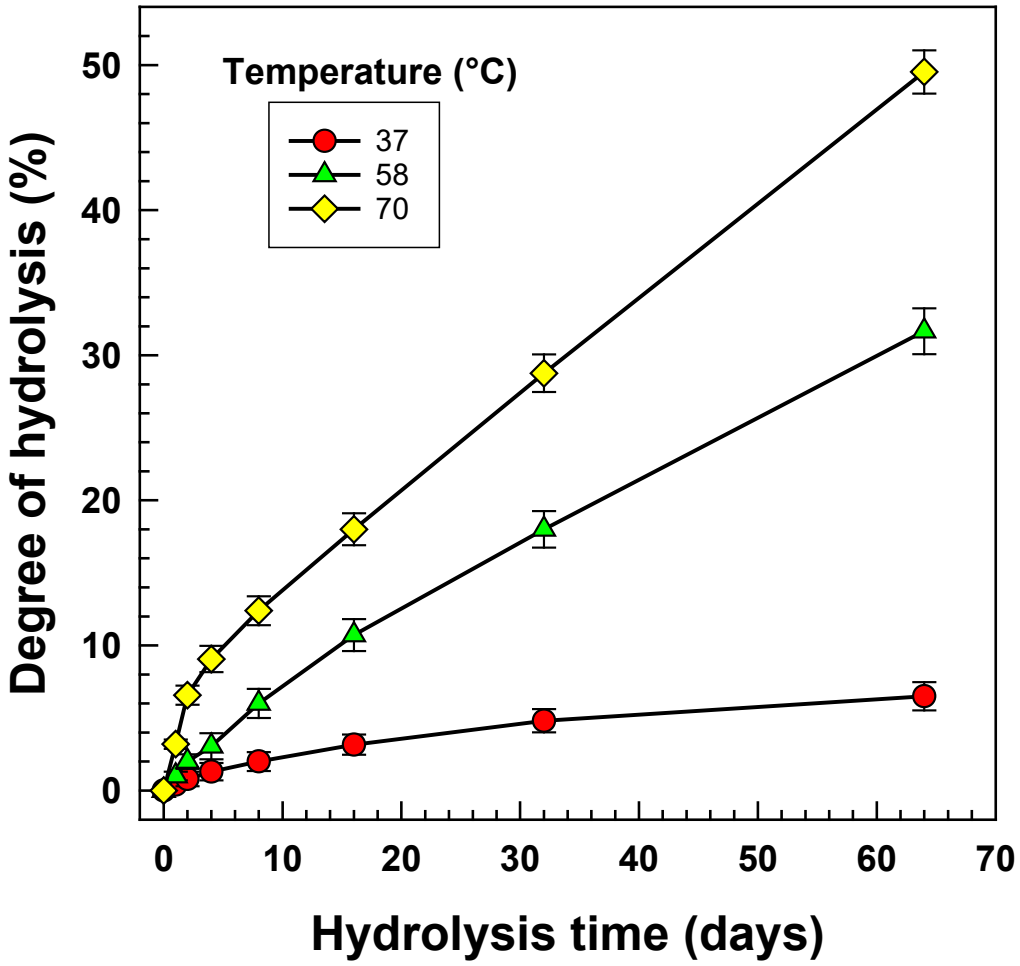

Figure 10. Degree of hydrolysis of PBSA during hydrolysis at various temperatures.

4. RESULTS AND DISCUSSION

Understanding the transformation of polymers during irradiation and hydrolysis relies not only on empirical observation but also on mathematical modeling. Analytical models enable researchers to extract quantitative information from experimental data and to predict the behavior of polymer systems under various conditions. This section presents the theoretical background of key models used to interpret cross-linking and crystallization processes.

To understand crystallization behavior in semicrystalline polymers such as PBSA, both isothermal and non-isothermal conditions were evaluated using various kinetic models. These models help to interpret the time and temperature dependence of crystallization, revealing insights into nucleation mechanisms, crystal growth, and thermal transitions.

4.1 Viscoelastic analysis in EVA

The viscoelastic response of EVA copolymers under shear deformation can be characterized using time-dependent creep compliance models. In semicrystalline polymers such as EVA, crystalline lamellae constrain amorphous chain mobility at room temperature, making it difficult to detect moderate levels of cross-linking. At elevated temperatures above the melting point (e.g. at 150 °C), these crystalline constraints are absent and the mechanical integrity of the material depends solely on the chemical cross-linked network. Therefore, high-temperature shear creep testing is a suitable approach to evaluate the cross-linking effect in such systems.

Shear deformation was preferred over tensile creep due to its higher sensitivity in detecting low cross-link densities. The experimental creep curves can be interpreted using classical viscoelastic models composed of idealized elements: springs representing elastic compliance (J) and dashpots representing viscosity (η). In this context, both four-parameter and six-parameter models are commonly applied to describe the full deformation and recovery process.

These models capture three key regimes of time-dependent behavior (see Figure 11): (i) instantaneous elastic deformation (J_0), (ii) delayed viscoelastic deformation represented by a Kelvin–Voigt element (J_1, η_1), and (iii) long-term viscous flow associated with irreversible strain (η_0). Upon unloading, immediate recovery occurs via the elastic spring, followed by a slower viscoelastic response. However, the viscous component leads to residual deformation, which reflects the permanent structural rearrangements within the material.

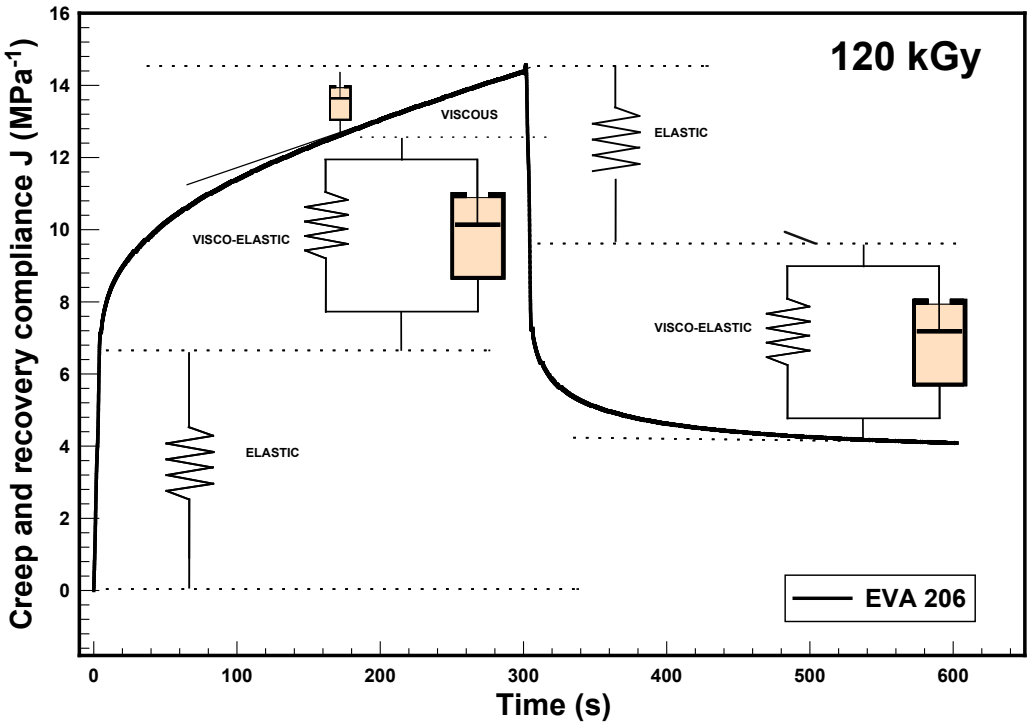

Figure 11. Creep compliance and recovery curve for experimental data of EVA 206-120 kGy with elastic, viscoelastic and viscous parts of the curve.

4.1.1 Four-parameter and six-parameter viscoelastic models

To analyze time-dependent deformation behavior under shear, four and six-parameter viscoelastic models were used to fit experimental creep curves. These models, based on combinations of elastic (spring) and viscous (dashpot) elements, allow for a detailed description of the material's response, including instantaneous deformation, delayed viscoelastic flow, and permanent strain. By applying these models, it is possible to extract characteristic mechanical parameters and compare the viscoelastic properties of different EVA copolymers as a function of irradiation dose. The four-parameter viscoelastic model used for creep analysis is depicted in Figure 12, with its mathematical representation provided in Equation 8. The six-parameter viscoelastic model is presented in Figure 13, with its mathematical formulation shown in Equation 9.

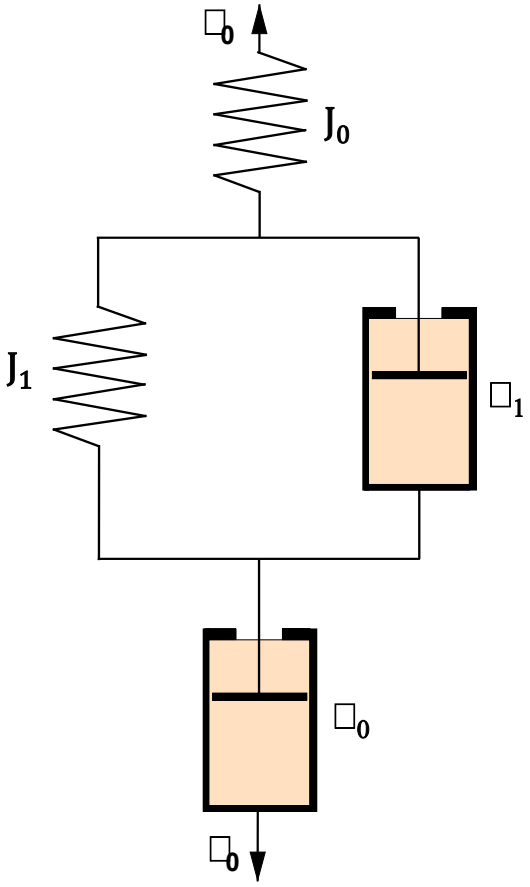

Figure 12. Four-element model for shear creep compliance (Burger model)

$$J(t) = J_0 + J_1\left(1 - e^{-\frac{t}{\lambda_1}}\right) + \frac{1}{\eta_0} \cdot t \qquad (8)$$

where
τ_0 = applied shear stress, Pa
t = time, s
J_0 = instantaneous shear compliance, Pa^{-1}
J_1 = retarded compliance, Pa^{-1}
η_0 = zero-shear or Newtonian viscosity, Pa.s
λ_1 = retardation time of retarded element $\lambda_1 = \frac{\eta_1}{G_1}$, s
η_1 = shear viscosity in viscoelastic region, Pa.s
G_1 = viscoelastic modulus of retarded element, Pa

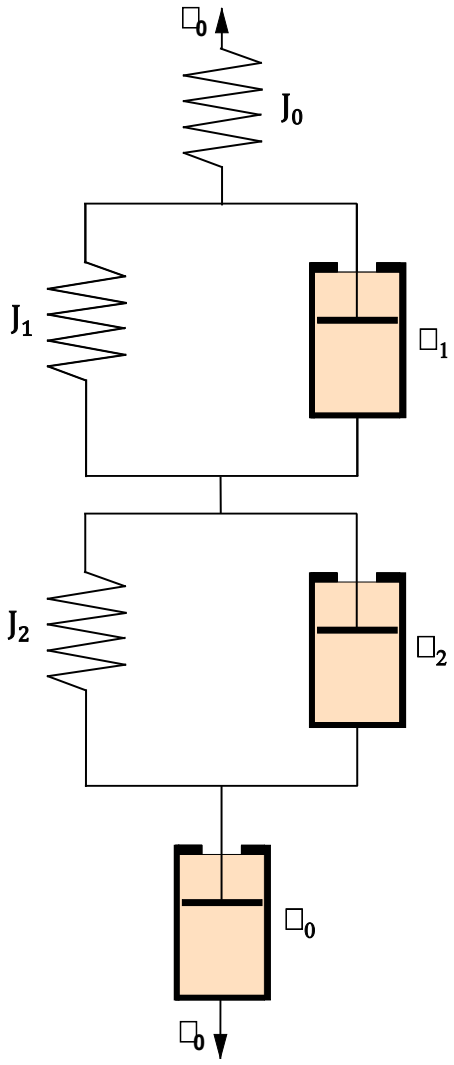

Figure 13. Six-element model for shear creep compliance.

More precise model of creep behavior contains six-parameters and is listed by Equation 9 [51].

$$J(t) = J_0 + J_1\left(1 - e^{-\frac{t}{\lambda_1}}\right) + J_2\left(1 - e^{-\frac{t}{\lambda_2}}\right) + \frac{1}{\eta_0}\cdot t \quad (9)$$

where

τ_0 = applied shear stress, Pa

t = time, s

J_0 = instantaneous shear compliance, Pa^{-1}

$J_1 \& J_2$ = retarded compliancies, Pa^{-1}

η_0 = zero-shear or Newtonian viscosity, Pa.s

$\lambda_1 \& \lambda_2$ = retardation times of retarded element $\lambda_1 = \frac{\eta_1}{G_1}$, $\lambda_2 = \frac{\eta_2}{G_2}$, s

$\eta_1 \& \eta_2$ = shear viscosities in viscoelastic region, Pa.s

$G_1 \& G_2$ = viscoelastic moduli of retarded element, Pa

4.2 Kinetics models

4.2.1 The Avrami analysis of isothermal crystallization

The Avrami equation is widely used to describe isothermal crystallization kinetics in semicrystalline polymers. It assumes that nucleation occurs randomly and independently within the sample and that crystal growth proceeds with a well-defined dimensionality over time. In 1940, Avrami [52] proposed a mathematical expression to describe the transformation process as follows:

$$X(t) = 1 - \exp(-K \cdot t^n) \quad (10)$$

where
$X(t)$ represents the relative crystallinity at a given time t,
K is a temperature-dependent rate constant,
n is the Avrami exponent, typically ranging from 1 to 4, which reflects the nature of nucleation and the dimensionality of crystal growth (e.g. linear, plate-like, and polyhedral development).

The Avrami equation is typically rearranged into a double logarithmic form to simplify data interpretation:

$$1 - X(t) = \exp(-K \cdot t^n) \quad (11)$$

$$ln[1 - X(t)] = -K \cdot t^n \quad (12)$$

$$-ln[1 - X(t)] = K \cdot t^n \quad (13)$$

$$log\{-ln[1 - X(t)]\} = \log K + n \cdot \log t \quad (14)$$

Isothermal crystallization typically results in a sigmoidal (S-shaped) curve when the degree of crystallinity is plotted against time. This reflects three stages of transformation: an initial induction period with slow nucleation, a region of accelerated crystal growth, and a final plateau as the system approaches completion.

Figure 14 illustrates the evolution of relative crystallinity during isothermal crystallization, shown as typical sigmoidal (S-shaped) curves ranging from 0 to 1. These curves were obtained by integrating heat flow data from DSC and reveal key differences between unhydrolyzed samples (Figure 14a) and samples hydrolyzed for 64 days (Figure 14b). Hydrolysis significantly accelerated crystallization kinetics: while unhydrolyzed samples crystallized in approximately 3000 seconds, hydrolyzed samples completed crystallization in roughly 300 seconds.

These curves served as the basis for evaluating crystallization kinetics using multiple approaches: the Avrami model, reciprocal half-time of crystallization $\left(1/\tau_{1/2}\right)$ and the slope at the inflection point. In Figure 14c, $log\{-ln[1-X(t)]\}$ is plotted against $\log(t)$ demonstrating the influence of crystallization temperature. The linear trend and shifting intercept $(\log K)$ indicate increasing crystallization rates with temperature. Figure 14d further summarizes these trends by plotting $(\log K)$ and the corresponding Avrami exponent n as a function of temperature. The values of n are close to 3, which suggests three-dimensional crystal growth.

Our findings are consistent with the study by Yang et al. [53], who reported similar behavior for biodegradable poly(ethylene adipate). They found that higher molecular weight samples exhibited longer half-times $\left(1/\tau_{1/2}\right)$ of crystallization and slightly higher Avrami exponents, with n ≈ 3 for both molecular weights studied at 35 °C.

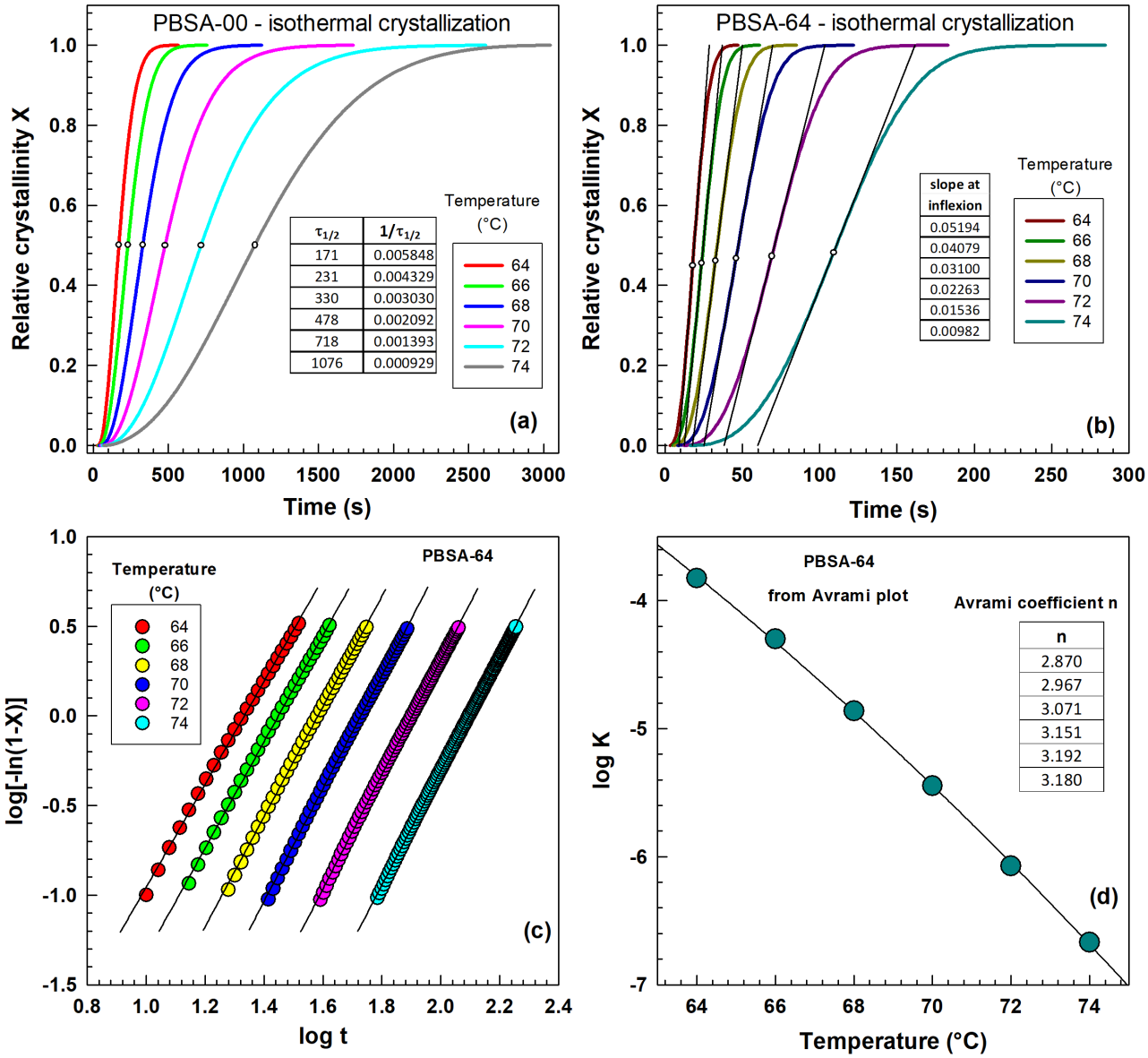

Figure 14. Influence of isothermal crystallization temperature on relative crystallinity curves from differential scanning calorimetry (DSC) for: (a) PBSA-00 sample (0 days of hydrolysis) and (b) PBSA-64 sample (64 days of hydrolysis at 70°C), (c) PBSA-64 sample (Avrami plot) and (d) PBSA-64 sample (Avrami rate constant K and exponent n).

4.2.2 Hoffman-Weeks method

The Hoffman-Weeks method is used to determine the equilibrium melting temperature (T_m^0) by extrapolating experimental melting temperatures against crystallization temperatures (T_c). The linear relationship observed allows prediction of ultimate thermal stability and serves as a benchmark for comparing crystallinity levels.

Figure 15a shows heat flow curves for PBSA samples crystallized at various temperatures (T_c). Each curve contains two melting peaks; the left-hand peak systematically shifts to higher temperatures with increasing (T_c). This peak was used for constructing of the Hoffman–Weeks plot presented in Figure 15b.

The equilibrium melting point (T_m^0) was estimated as the intersection of the linear regression line through experimental data with the reference line $T_m = T_c$ [54] yielding a value of 135.42 °C. This value was subsequently used in the Gibbs–Thomson and Hoffman–Lauritzen analyses. Our findings are in good agreement with results published by Zhao et al. [55] on poly(butylene succinate-co-adipate) blends and Wang et al. [56] on the melting behavior of poly(butylene succinate-adipate).

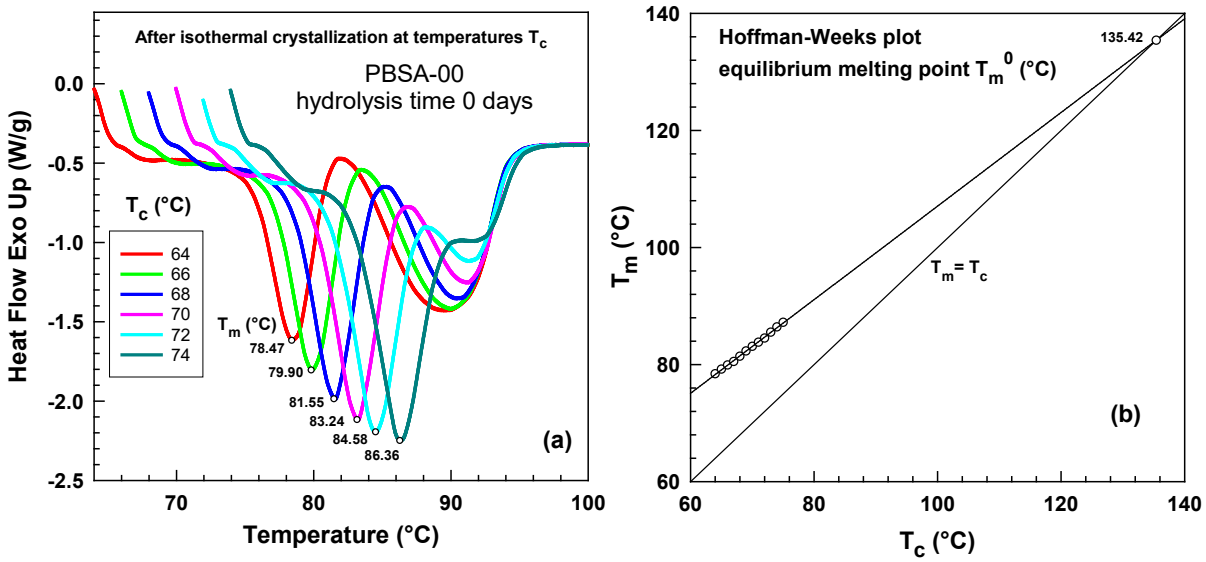

Figure 15. Heat flow curves during the heating experiment at rate 20°C/min after isothermal crystallization at various temperatures: (a) PBSA hydrolysis time 0 days, (b) Hoffman-Weeks plot for PBSA hydrolysis time 0 days.

4.2.3 Hoffman-Lauritzen Theory

The Hoffman–Lauritzen theory provides a framework for describing the temperature dependence of crystallization rates in semicrystalline polymers. It is particularly useful in the range between the glass transition temperature (T_g) minus 30 K and the equilibrium melting temperature (T_m^0). This semi-empirical model describes the temperature dependence of spherulitic growth rates (G) in polymers [57]:

$$G = G_0 \, exp\left[\frac{-U^*}{R(T_c - T_\infty)} - \frac{K_g}{T_c(\Delta T)f}\right] \qquad (15)$$

where
G is the crystals growth rate;
U^* is a constant (1500 cal mol^{-1}) representing the activation energy required for chains to move repeatedly;
R is the gas constant 8.314 J K^{-1} mol^{-1};
T_c is the crystallization temperature in Kelvin;
T_∞ is defined as T_g-30K, where T_g is the glass transition temperature (for PBSA, $T_g = 230\ K$), $T_\infty = 200K$;
ΔT is the undercooling, calculated as $T_m^0 - T_c$;
T_m^0 is the equilibrium melting temperature of an infinitely thick crystal, for PBSA $T_m^0 = 408.57K$;
K_g is the nucleation constant;
f is a correction factor, equal to $2T_c/(T_m^0 + T_c)$;
G_0 is a pre-exponential factor.

For the evaluation of DSC data, the crystallization rate constant (G) was substituted by the inverse of the half-time of crystallization $(1/\tau_{1/2})$. Equation 16 was used to construct the linear plots shown in Figure 16a, where the slope corresponds to the (K_g) parameter and the intercept $ln(G_0)$ was used to generate Figure16b.

$$ln\left(\frac{1}{\tau_{1/2}}\right) + \frac{U^*}{R(T_c - T_\infty)} = ln\, G_0 - \frac{K_g}{T_c \Delta T f} \qquad (16)$$

Figure 16a shows fitted lines for PBSA samples subjected to 0, 16, 32, and 64 days of hydrolysis. Within the narrow temperature intervals examined, the data exhibit near-linear behavior, enabling the extraction of slope and intercept values for each hydrolysis condition. These slopes correspond to the activation energy for transport across the phase boundary, while the intercept relates to the pre-exponential factor $ln(G_0)$. Figure 16b presents the evolution of $ln(G_0)$, which

increases with hydrolysis time and was fitted using an exponential rise-to-maximum function. Figure 16c depicts the reciprocal half-time of crystallization $1/\tau_{1/2}$ as a function of temperature. The maximum crystallization rate was observed around the midpoint between $T_g - 30$ and T_m^0 consistent with the predictions of Hoffman–Lauritzen theory.

Our results align well with the findings of Si and Luo [58], who investigated PBSA/thiodiphenol complexes, and Qiu and Qiu [59], who studied crystallization kinetics of poly(ethylene suberate).

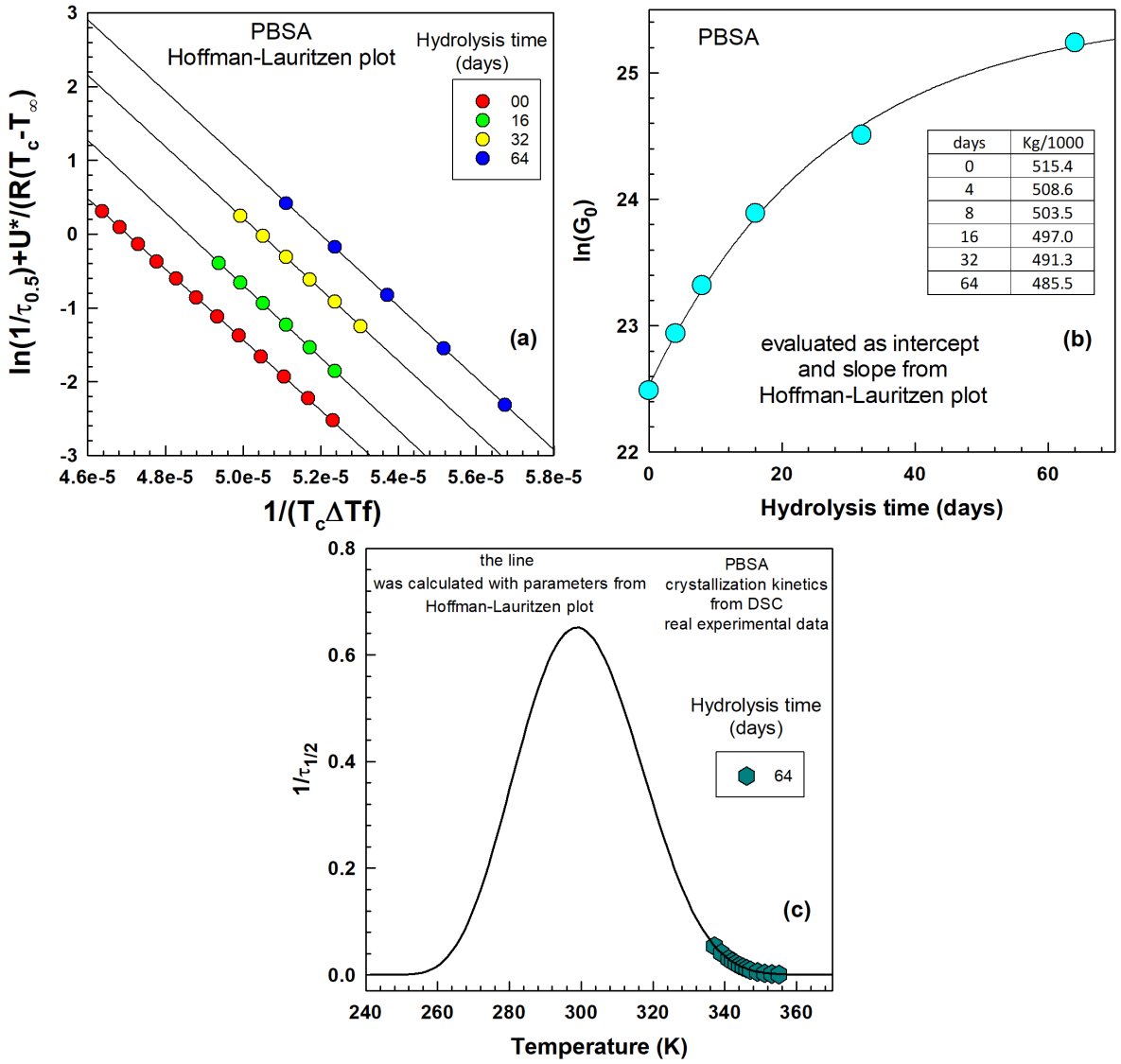

Figure 16. (a) Hoffman-Lauritzen plot for PBSA after 00, 16, 32, 64 days of hydrolysis, (b) pre-exponential factor $\ln(G_0)$ as a function of hydrolysis time, (c) reciprocal half-time of crystallization $1/\tau_{1/2}$ as a function of temperature in K.

4.2.4 Gibbs-Thomson Equation

Changes in lamellar thickness during crystallization can be described using the Gibbs–Thomson equation, which relates melting temperature (T_m) to the dimensions of crystalline lamellae l:.

The general form of the equation is [60]:

$$T_m(l) = T_m^0\left(1 - \frac{2}{\Delta h}\left(\frac{\sigma}{a} + \frac{\sigma}{b} + \frac{\sigma_e}{l}\right)\right) \quad (17)$$

where

$T_m(l)$ is melting temperature of lamellar crystal;
T_m^0 is the equilibrium melting temperature;
σ is the surface free energy;
σ_e is the end surface free energy;
Δh is the heat of fusion;
a is a lateral size of lamellae;
b is a lateral size of lamellae;
l is thickness of lamellar.

Since a and b are typically much larger than l, Equation 17 can be simplified to:

$$T_m(l) = T_m^0 - \frac{C}{l}, \qquad \text{where} \quad C = \frac{2\sigma_e T_m^0}{\Delta h} \quad (18)$$

The relative change in lamellar thickness can then be estimated from melting temperatures using:

$$\frac{l_2}{l_1} = \frac{T_m^0 - T_{m1}(l)}{T_m^0 - T_{m2}(l)} \quad (19)$$

In this study, T_m^0 was determined from the Hoffman–Weeks plot (Figure 15b). Applying Equation 19 yielded an estimated lamellar thickness after 64 days of hydrolysis ratio of: $l_2/l_1 = (135.42 - 92.5)/(135.42 - 98) = 1.147$.

The equation helps in evaluating crystal size and understanding morphological changes induced by degradation. Together, these models offer a multifaceted theoretical framework for interpreting experimental data, enabling a deeper understanding of polymer transformation mechanisms under irradiation and hydrolysis.

4.2.5 The Jeziorny anylysis of non-isothermal crystallization

To describe non-isothermal crystallization kinetics, Jeziorny modified the original Avrami model to account for varying temperature. This method applies the Avrami equation to DSC data recorded during cooling and introduces a correction factor that considers the effect of the cooling rate on crystallization kinetics. The result is a crystallization rate constant Z_c that enables kinetic interpretation under dynamic thermal conditions.

The original Avrami equation under non-isothermal conditions is expressed as:

$$X(t) = 1 - \exp(-Z_t \cdot t^n) \quad (20)$$

Rearranged forms used in linearization are:

$$1 - X(t) = \exp(-Z_t \cdot t^n) \quad (21)$$

$$ln[1 - X(t)] = -Z_t \cdot t^n \quad (22)$$

$$-ln[1 - X(t)] = Z_t \cdot t^n \quad (23)$$

$$log\{-ln[1 - X(t)]\} = \log Z_t + n \cdot \log t \quad (24)$$

In these expressions, n is the Avrami exponent, which reflects nucleation type and growth dimensionality, and Z_t is the crystallization rate constant under non-isothermal conditions.

To compensate for the influence of different cooling rates, Jeziorny proposed a correction to the rate constant Z_t as follows:

$$\log Z_c = \frac{\log Z_t}{\phi} \quad (25)$$

where Z_c s the corrected crystallization rate constant and ϕ is the cooling rate. Although originally formulated for isothermal conditions in low-molecular-weight substances, the Avrami model has been extensively applied to non-isothermal crystallization of polymers. Under these dynamic thermal conditions, the Avrami parameters n and Z_t lose their strict physical meaning but remain useful for comparing crystallization trends and assessing the influence of processing conditions or chemical modification [61]. The theoretical interpretation of the exponent n is sometimes guided by the following relation [62]:

$$n = \alpha + \frac{d}{p} \quad (26)$$

where:

α is the nucleation index (1 for homogeneous, 0 for heterogeneous nucleation),

d is the dimensionality of growth (1, 2, or 3),

p is the growth mechanism index (1 for interface-controlled, 0.5 for diffusion-controlled growth).

Despite the limitations, Jeziorny's adaptation of the Avrami model remains a widely accepted method for the kinetic analysis of polymer crystallization under realistic processing conditions.

Figure 17a presents the crystallization rate constant Z_t as a function of hydrolysis time. The results indicate a steady increase in growth rate with hydrolysis, showing an approximately linear trend up to 16 days. Figure 17b depicts the dependence of Z_t on cooling rate, revealing a consistent upward trend. The corrected crystallization rate constant Z_c calculated according to Equation 25, also increases with cooling rate. These findings are consistent with previous studies, including Bandyopadhyay and Ray [63], who reported a similar trend for polypropylene/PBSA blends, and Chen et al. [64], who observed comparable behavior in poly(3-hydroxybutyrate) (PHB).

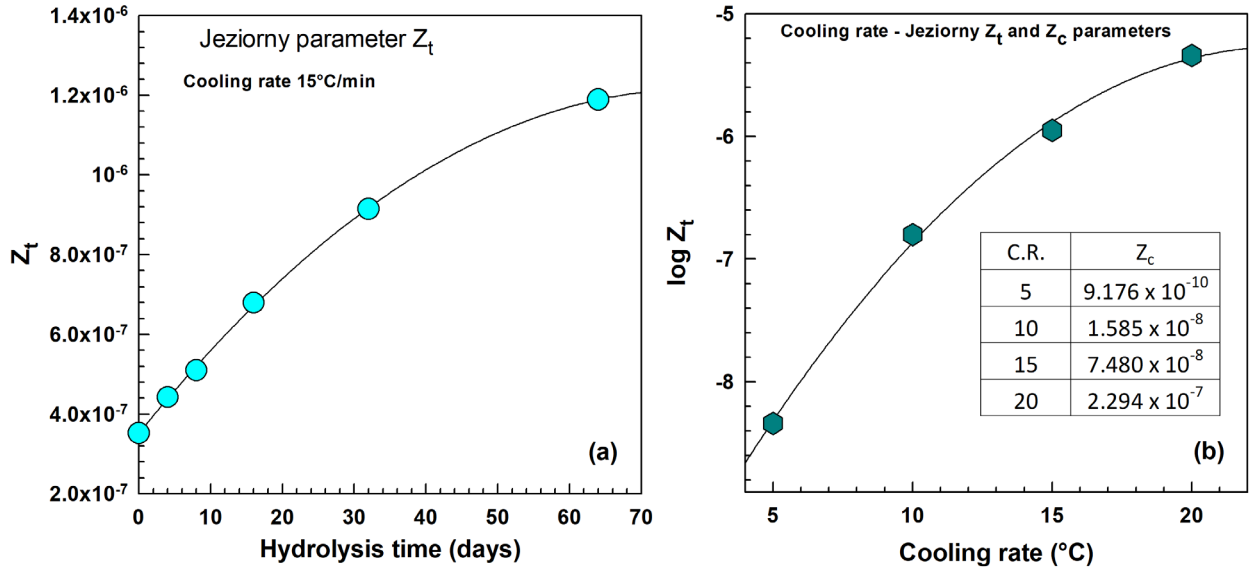

Figure 17. Plot of Jeziorny's parameter Z_t from Avrami plot. (a) as a function of hydrolysis times at cooling rate 15 °C/min, (b) PBSA after 32 days of hydrolysis at 70 °C as a function of cooling rate.

4.2.1 Ozawa analysis of non-isothermal crystallization

The Ozawa model is widely used to analyze non-isothermal crystallization behavior by describing the dependence of relative crystallinity on temperature and cooling rate. The model assumes that the overall crystallization process can be represented by a temperature dependent crystallization function $K(T)$, a cooling rate ϕ and exponent m, which reflects the mechanism and dimensionality of crystal growth.

The general form of the Ozawa equation is [65]:

$$X = 1 - e^{\left[\frac{-K(T)}{\phi^m}\right]} \quad (27)$$

where:
X is relative crystallinity in range 0–1,
ϕ is the cooling rate,
m is the Ozawa exponent,
$K(T)$ is a temperature-dependent function related to crystallization rate.

For quantitative evaluation, a double-logarithmic form of the equation is often used:

$$\log[-ln(1 - X)] = \log K(T) - m \log \phi \quad (28)$$

Plotting $\log[-ln(1 - X)]$ versus $\log \phi$ enables the determination of Ozawa parameters m and $K(T)$. This method provides valuable insights into how cooling rate influences crystallization kinetics, which is particularly important for processing and for evaluating structural changes due to degradation or modification.

The Ozawa exponent m plays a role analogous to the Avrami exponent n under isothermal conditions. It reflects the dimensionality of crystal growth:
$m = 1$ suggest one-dimensional (needle-like or rod-shaped crystals) growth,
$m = 2$ correspond to two-dimensional (plate-like or disc-shaped) growth,
$m = 3$ is indicative of three-dimensional (spherulitic) structures.

Figure 18a shows Avrami plots for PBSA samples with varying hydrolysis durations. The curves corresponding to 0–16 days are closely grouped, while those for 32 and 64 days exhibit noticeable separation, indicating substantial changes in crystallization kinetics due to hydrolysis. The intercepts of these plots allow the determination of Jeziorny's crystallization rate constant Z_t.

Figure 18b presents Avrami plots for samples hydrolyzed for 32 days under different cooling rates. The plots for 10, 15, and 20 °C/min are closely aligned, whereas the curve for 5 °C/min deviates more significantly, suggesting a pronounced change in crystallization behavior at slower cooling. These trends are consistent with the findings of Jiang et al. [66], who studied PBS/PBSA blends under similar conditions.

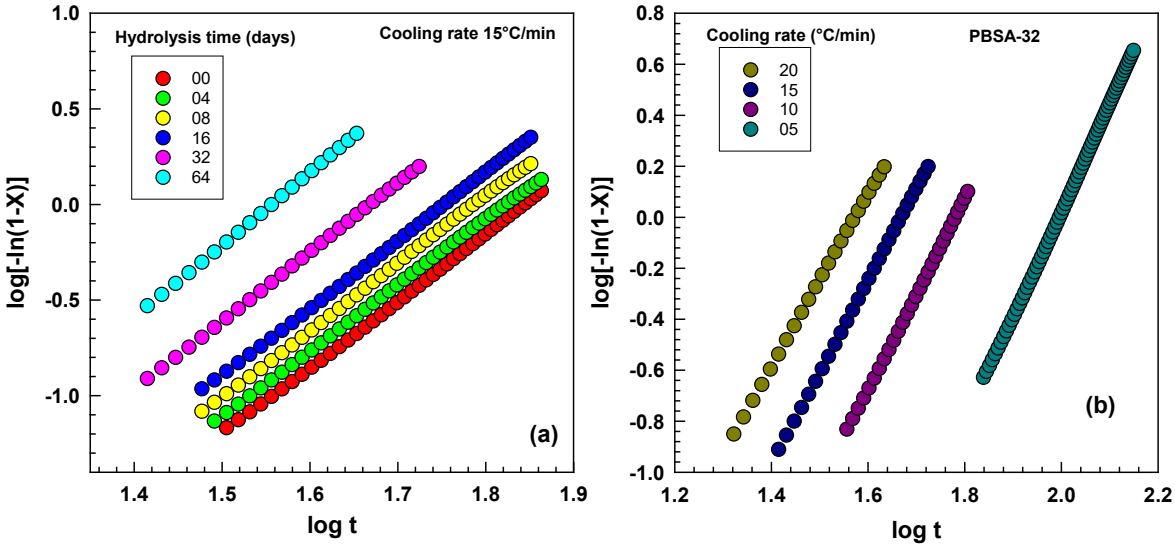

Figure 18. Avrami plot from DSC. (a) for various hydrolysis times at cooling rate 15 °C/min, (b) PBSA after 32 days of hydrolysis at 70 °C for various cooling rates (5–20 °C/min).

Numerous studies [67-72] have employed Ozawa analysis to characterize non-isothermal crystallization of semicrystalline polymers. For accurate results, the use of closely spaced cooling rates is recommended to ensure linearity of the log–log plot.

Figure 19a presents the Ozawa exponent m, which reflects nucleation and crystal growth mechanisms. The parameter ranges from approximately 2.2 to 3.2 and shifts toward higher temperatures with increasing hydrolysis time. A gradual increase in m is observed at higher temperatures, and its overall range expands with hydrolysis e.g., from 2.4-3.0 at 0 days to 2.8-3.2 at 64 days indicating changes in the crystallization mechanism.

Figure 19b displays the Ozawa cooling function $K(T)$ for PBSA samples with varying degrees of hydrolysis. This function defines both the effective crystallization temperature range and the rate of crystallization. A shift in crystallization to higher temperatures is evident following hydrolysis, and samples hydrolyzed for 16, 32, and 64 days exhibited higher $K(T)$ values compared to those hydrolyzed for shorter durations (0, 4, and 8 days), confirming an enhancement in crystallization kinetics with hydrolysis progression.

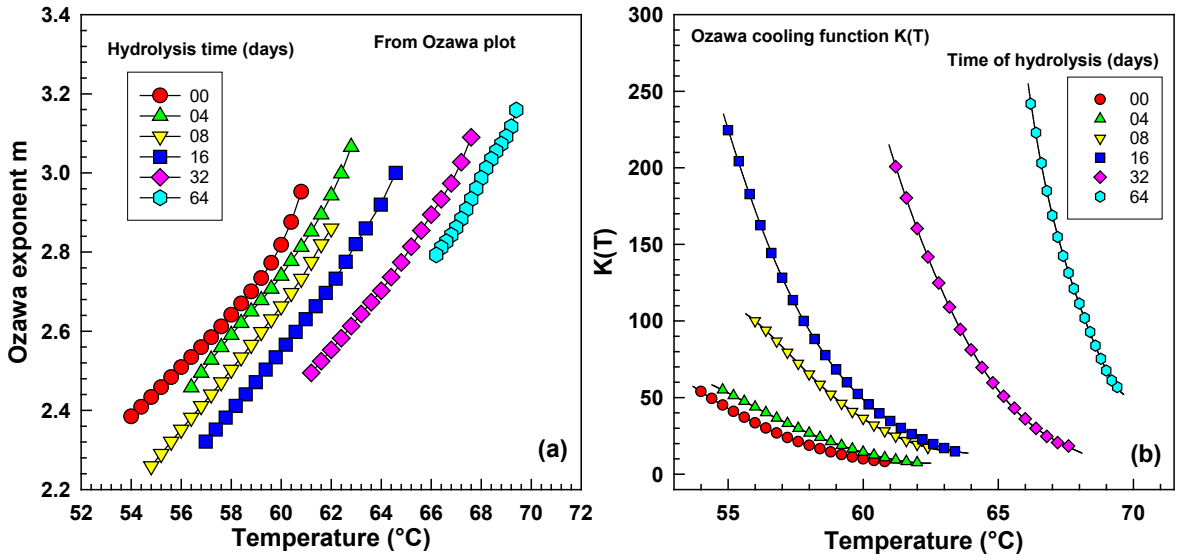

Figure 19. Detailed analysis of Ozawa parameters (a) Ozawa exponent m for PBSA, (b) Ozawa cooling function.

4.2.2 Kratochvíl Method

The Kratochvíl method is a model independent approach used to evaluate crystallization behavior under dynamic conditions. Unlike model-based methods (e.g. Avrami or Ozawa), it does not rely on assumptions about nucleation mechanisms or growth geometry. Instead, it focuses on geometrical and derivative analysis of the crystallization curve obtained by DSC.

Originally proposed by Kratochvíl and Kelnar [73], the method evaluates the crystallization rate based on the slope of the relative crystallinity curve at its inflection point. This inflection point corresponds to the maximum crystallization rate, typically located near the midpoint of the transformation ($X \approx 0.5$). Although this slope does not have a strict kinetic interpretation, it is a useful empirical indicator of crystallization behavior, particularly for comparing samples with structural modifications. In our modified version of the Kratochvíl method, the slope was determined from plots of relative crystallinity versus time rather than temperature. This refinement enhances the temporal resolution of the crystallization process and allows for direct comparison with other time-based kinetic indicators such as the half-time of crystallization $(\tau_{1/2})$. As demonstrated in our study on hydrolyzed PBSA, the slope at the inflection point decreased with progressing hydrolysis, reflecting faster crystallization. This trend was consistent across all cooling rates (5, 10, 15, and 20 °C/min) and was further confirmed by analyses using the modified Avrami equation and half-time crystallization $(\tau_{1/2})$. All three methods revealed similar trends, supporting the validity of the slope-based approach for assessing crystallization kinetics under non-isothermal conditions.

Figure 20a illustrates the evolution of relative crystallinity over time, shown as characteristic sigmoidal (S-shaped) curves. As hydrolysis progressed, the total crystallization time decreased, likely due to a reduced amorphous phase fraction. To evaluate crystallization kinetics, a modified version of the Kratochvíl method was applied, in which the slope at the inflection point of the relative crystallinity vs. time curve was used as a measure of crystallization rate. This slope carries a direct kinetic interpretation and it effectively reflects relative changes in crystallization kinetics.

In addition to this approach, crystallization kinetics were also assessed using the modified Avrami equation and the reciprocal half-time of crystallization. All three methods showed consistent trends—an increase in crystallization rate with increasing hydrolysis time, across all tested cooling rates (5, 10, 15, and 20 °C/min).

Figure 20b shows the slope at the inflection point plotted as a function of hydrolysis time. The crystallization rate increased nearly linearly with hydrolysis duration under all cooling conditions. These results are in good agreement with findings from previous studies.

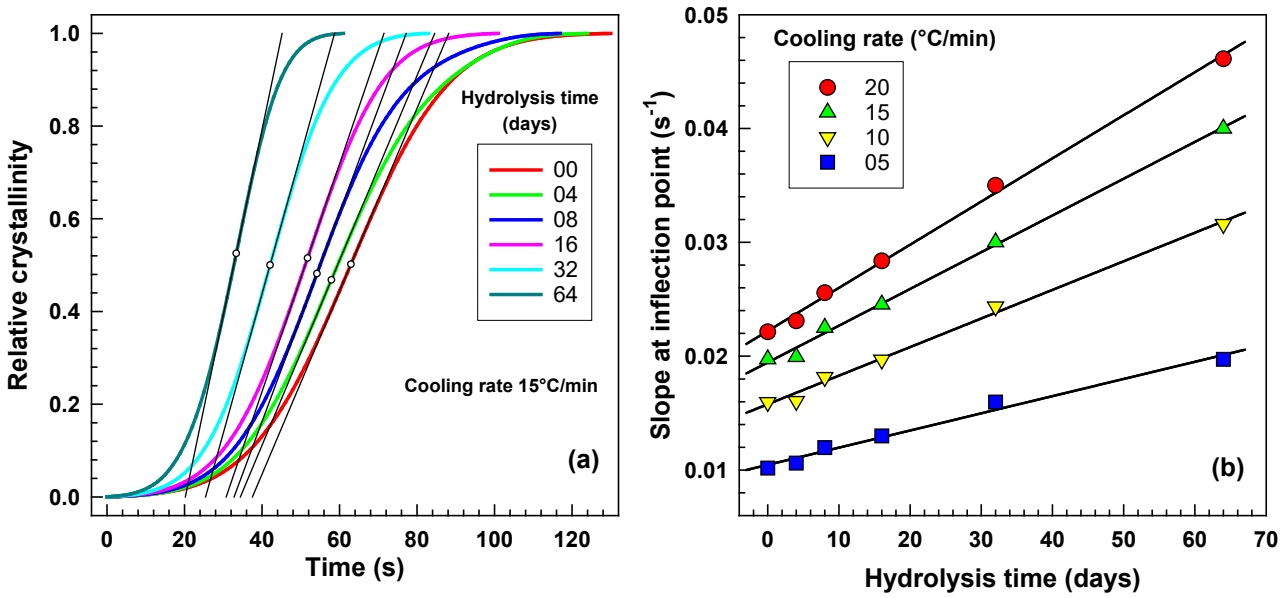

Figure 20. Crystallization kinetics from DSC. (a) relative crystallinity vs. time, (b) slope at the inflection point vs. time of hydrolysis.

SUMMARY OF WORK AND CONTRIBUTION TO SCIENCE AND PRACTICE

This doctoral thesis summary provides a theoretical and experimental framework for understanding two significant pathways of polymer modification: radiation cross-linking and hydrolytic degradation. Through a detailed investigation of ethylene vinyl acetate (EVA) and poly(butylene succinate-co-adipate) (PBSA) copolymers, the work contributes to the following:

- Consolidation of knowledge on electron beam-induced cross-linking in polyolefinic materials, emphasizing the role of vinyl acetate content in network formation and stability.
- Clarification of degradation mechanisms in biodegradable polyesters under hydrolytic conditions, focusing on time- and temperature-dependent changes in crystallinity and lamellar structure.
- Expansion of analytical models and methods, including the use of Avrami, Charlesby-Pinner, Ozawa, and Hoffman–Lauritzen frameworks to interpret data from thermal and mechanical analyses.
- Establishment of structure–property relationships linking molecular modifications with changes in viscoelasticity, crystallization kinetics, and thermal behavior. into how structural modifications at the molecular level influence macroscopic properties such as viscoelasticity, and crystallization kinetics.

These findings are highly relevant to the rational design of polymers with tailored performance whether for durable technical applications such as cable insulation, or biodegradable systems intended for composting and controlled degradation. The thesis lays a solid foundation for further research combining theoretical modeling with practical implementation in sustainable polymer systems.

CONCLUSION

This doctoral thesis summary presents an in-depth investigation into the effects of electron beam irradiation and hydrolytic degradation on the structural and functional behavior of selected copolymers specifically ethylene vinyl acetate (EVA) and poly(butylene succinate-co-adipate) (PBSA). The work integrates experimental analysis with theoretical modeling to evaluate how cross-linking and hydrolysis affect crystallization, viscoelastic behavior, and molecular architecture.

For EVA copolymers, the study demonstrated that electron beam irradiation leads to progressive cross-linking, with higher vinyl acetate content resulting in a more efficient network formation. Gel content analysis confirmed dose-dependent behavior, and advanced techniques such as DMA, Charlesby-Pinner and Charlesby-Rosiak equations, and rheological models provided comprehensive insight into cross-link density evolution. Additionally, complex modulus measurements at elevated temperatures revealed the dominance of cross-linking effects over chain scission in determining viscoelastic properties.

For PBSA, the study focused on the influence of hydrolysis on crystallization kinetics, morphology, and molar mass degradation. Isothermal and non-isothermal DSC experiments analyzed using the Avrami, Jeziorny, Ozawa, and Kratochvíl approaches, revealed accelerated crystallization with increasing hydrolysis time. The Hoffman–Weeks and Gibbs–Thomson methods enabled evaluation of lamellar structure changes, while hydrolysis conditions at varying temperatures demonstrated strong temperature-dependent degradation behavior.

The research contributes to the scientific understanding of how radiation and hydrolysis alter the structure–property relationships of biodegradable and semicrystalline copolymers. These findings are relevant for applications in sustainable materials, cable insulation, packaging, and biomedical fields where controlled degradation is required.

REFERENCES

[1] Turgis JD, Verge C, Coqueret X. Composition effects on the EB-induced cross-linking of some acrylate and methacrylate copolymers. Radiation Physics and Chemistry. 2003;67(3-4):409-413. https://doi.org/10.1016/S0969-806x(03)00076-8.

[2] Kolhe A, Chauhan A, Dongre A. A Review on various methods for the Cross-linking of Polymers. Research Journal of Pharmaceutical Dosage Forms and Technology. 2022:183-188. https://doi.org/10.52711/0975-4377.2022.00029.

[3] Clegg DW. Irradiation effects on polymers. London, United Kingdom: Elsevier Applied Science; 1991.

[4] Ries MD, Pruitt L. Effect of cross-linking on the microstructure and mechanical properties of utra-high molecular weight polyethylene. Clinical Orthopaedics and Related Research. 2005(440):149-156. https://doi.org/10.1097/01.blo.0000185310.59202.e5.

[5] Makuuchi K, Cheng S. Radiation Processing of Polymer Materials and Its Industrial Applications. Hoboken, New Jersey: John Wiley & Sons, Inc.; 2012.

[6] Giselly M. G. Farias PA, Ruth B. L. Hanken, Jeane P. de Araújo, Akidauana D. B. de Oliveira & Tomás J. A. de Mélo. Effect of EVA copolymer containing different VA content on the thermal and rheological properties of bio-based high-density polyethylene/ethylene vinyl acetate blends. Journal of Thermal Analysis and Calorimetry. 2021;146. https://doi.org/10.1007/s10973-020-10423-5.

[7] Wang B, Wang MH, Xing Z, Zeng HY, Wu GZ. Preparation of radiation crosslinked foams from low-density polyethylene/ethylene-vinyl acetate (LDPE/EVA) copolymer blend with a supercritical carbon dioxide approach. Journal of Applied Polymer Science. 2013;127(2):912-918. https://doi.org/10.1002/app.37826.

[8] El Fray M, Przybytniak G, Piatek-Hnat M, Kornacka EM. Physical effects of radiation processes in poly(aliphatic/aromatic-ester)s modified with e-beam radiation. Polymer. 2010;51(5):1133-1139. https://doi.org/10.1016/j.polymer.2010.01.028.

[9] Ahmed J, Mushtaq S. Bridging the future: unveiling the latest innovations in ethylene vinyl acetate blends and composites through electron beam irradiation-a comprehensive review. Macromolecular Research. 2024;32(11):1049-1063. https://doi.org/10.1007/s13233-024-00292-4.

[10] Sabet M, Soleimani H, Hassan A, Ratnam CT. The Effect of Addition EVA and LDPE-g-MAH on Irradiated LDPE Filled with Metal Hydroxides. Polymer-Plastics Technology and Engineering. 2014;53(8):775-783. https://doi.org/10.1080/03602559.2014.886041.

[11] Sabet M, Hassan A, Wahit MU, Ratnam CT. Mechanical, Thermal and Electrical Properties of Ethylene Vinyl Acetate Irradiated by an Electron-Beam. Polymer-Plastics Technology and Engineering. 2010;49(6):589-594. https://doi.org/10.1080/03602551003652755.

[12] Gheysari D, Behjat A. The effect of high-energy electron beam irradiation and content of ATH upon mechanical and thermal properties of EVA copolymer. European Polymer Journal. 2002;38(6):1087-1093. https://doi.org/10.1016/S0014-3057(01)00281-6.

[13] Rezaeian I, Jafari SH, Zahedi P, Ghaffari M, Afradian S. Improvements of physical and mechanical properties of electron beam irradiation-crosslinked EVA foams. Polymers for Advanced Technologies. 2009;20(5):487-492. https://doi.org/10.1002/pat.1298.

[14] Kim DW, Kim KS. Electron beam irradiation of noncrosslinked LDPE-EVA foam. Journal of Cellular Plastics. 2002;38(6):471-496. https://doi.org/10.1177/002195502128791279.

[15] Allan JM, Mumin MA, Xu WZ, Al Sharari Q, Charpentier PA. Surface functionalized bare and core-shell quantum dots in poly (ethylene-co-vinyl acetate) for light selective nanocomposite films. Solar Energy Materials and Solar Cells. 2014;123:30-40. https://doi.org/10.1016/j.solmat.2013.12.007.

[16] Hirschl C, Biebl-Rydlo M, DeBiasio M, Muhleisen W, Neumaier L, Scherf W, Oreski G, Eder G, Chernev B, Schwab W, Kraft M. Determining the degree of crosslinking of ethylene vinyl acetate photovoltaic module encapsulants-A comparative study. Solar Energy Materials and Solar Cells. 2013;116:203-218. https://doi.org/10.1016/j.solmat.2013.04.022.
[17] Sen M, Guven O. A Comparative-Study of Thermal and Mechanical Stabilities of Gamma-Irradiated Ethylene-Ethyl Acrylate and Ethylene-Vinyl Acetate Copolymers. Radiation Physics and Chemistry. 1995;46(4-6):871-874. https://doi.org/10.1016/0969-806x(95)00281-2.
[18] Matsui T, Shimoda M, Osajima Y. Mechanical Changes of Electron-Beam Irradiated Ethylene Vinyl-Acetate Copolymer (Eva) Film .1. Polymer International. 1992;29(2):85-90. https://doi.org/10.1002/pi.4990290204.
[19] Nicholson L, Whitley K, Gates T. The Role of Molecular Weight and Temperature on the Elastic and Viscoelastic Properties of a Glassy Thermoplastic Polyimide. International Journal of Fatigue. 2002;24:185-195. https://doi.org/10.1016/S0142-1123(01)00072-X.
[20] Rodriguez EJ, Marcos B, Huneault MA. Hydrolysis of polylactide in aqueous media. Journal of Applied Polymer Science. 2016;133(44). https://doi.org/10.1002/app.44152.
[21] Baidurah S, Takada S, Shimizu K, Ishida Y, Yamane T, Ohtani H. Evaluation of biodegradation behavior of poly(butylene succinate-co-butylene adipate) with lowered crystallinity by thermally assisted hydrolysis and methylation-gas chromatography. Journal of Analytical and Applied Pyrolysis. 2013;103:73-77. https://doi.org/10.1016/j.jaap.2012.08.011.
[22] Tsuji H, Shimizu K, Sato Y. Hydrolytic degradation of poly(L-lactic acid): Combined effects of UV treatment and crystallization. Journal of Applied Polymer Science. 2012;125(3):2394-2406. https://doi.org/10.1002/app.36498.
[23] Marten E, Müller RJ, Deckwer WD. Studies on the enzymatic hydrolysis of polyesters I.: Low molecular mass model esters and aliphatic polyesters. Polymer Degradation and Stability. 2003;80(3):485-501. https://doi.org/10.1016/S0141-3910(03)00032-6.
[24] Seo KS, Cloyd JD. Kinetics of Hydrolysis and Thermal-Degradation of Polyester Melts. Journal of Applied Polymer Science. 1991;42(3):845-850. https://doi.org/10.1002/app.1991.070420330.
[25] Palai B, Mohanty S, Nayak SK. A Comparison on Biodegradation Behaviour of Polylactic Acid (PLA) Based Blown Films by Incorporating Thermoplasticized Starch (TPS) and Poly (Butylene Succinate-co-Adipate) (PBSA) Biopolymer in Soil. Journal of Polymers and the Environment. 2021;29(9):2772-2788. https://doi.org/10.1007/s10924-021-02055-z.
[26] Bai ZH, Shi K, Su TT, Wang ZY. Correlation between the chemical structure and enzymatic hydrolysis of Poly(butylene succinate), Poly(butylene adipate), and Poly(butylene suberate). Polymer Degradation and Stability. 2018;158:111-118. https://doi.org/10.1016/j.polymdegradstab.2018.10.024.
[27] Bikiaris DN, Papageorgiou GZ, Achilias DS. Synthesis and comparative biodegradability studies of three poly(alkylene succinate)s. Polymer Degradation and Stability. 2006;91(1):31-43. https://doi.org/10.1016/j.polymdegradstab.2005.04.030.
[28] La Fuente CIA, Maniglia BC, Tadini CC. Biodegradable polymers: A review about biodegradation and its implications and applications. Packaging Technology and Science. 2023;36(2):81-95. https://doi.org/10.1002/pts.2699.
[29] Vyazovkin S, Sbirrazzuoli N. Nonisothermal Crystallization Kinetics by DSC: Practical Overview. Processes2023.
[30] Yang X, Yu B, Sun H, Wang N, Liu P, Feng J, Cui X. Isothermal and Non-Isothermal Crystallization Kinetics of Poly(ethylene chlorotrifluoroethylene). Polymers2022.
[31] Pérez E, Angulo I, Blázquez-Blázquez E, Cerrada ML. Characteristics of the Non-Isothermal and Isothermal Crystallization for the β Polymorph in PVDF by Fast Scanning Calorimetry. Polymers2020.

[32] ASTM D2765-16: Standard Test Methods for Determination of Gel Content and Swell Ratio of Crosslinked Ethylene Plastics. West Conshohocken, PA: ASTM International; 2024.
[33] Salehi SMA, Mirjalili G, Amrollahi J. Effects of high-energy electron beam on low-density polyethylene materials containing EVA. Journal of Applied Polymer Science. 2004;92(2):1049-1052. https://doi.org/10.1002/app.20079.
[34] Wang SF, Zhang Y, Zhang YX, Zhang CM, Li EJ. Crosslinking of polyvinyl chloride by electron beam irradiation in the presence of ethylene-vinyl acetate copolymer. Journal of Applied Polymer Science. 2004;91(3):1571-1575. https://doi.org/10.1002/app.13265.
[35] Datta SK, Bhowmick AK, Tripathy DK, Chaki TK. Effect of electron beam radiation on structural changes of trimethylol propane trimethacrylate, ethylene vinyl acetate, and their blends. Journal of Applied Polymer Science. 1996;60(9):1329-1341. https://doi.org/10.1002/(SICI)1097-4628(19960531)60:9<1329::AID-APP8>3.0.CO;2-L.
[36] Ali ZI, Legocka I. Effect of metal salt of ethylene/methacrylic acid copolymer on electron beam crosslinking of low density polyethylene. Advances in Polymer Technology. 2005;24(2):103-113. https://doi.org/10.1002/adv.20034.
[37] Manaila E, Craciun G, Ighigeanu D, Lungu IB, Dumitru M, Stelescu MD. Electron Beam Irradiation: A Method for Degradation of Composites Based on Natural Rubber and Plasticized Starch. 2021;13(12):1950. https://doi.org/10.3390/polym13121950.
[38] Anagha MG, Chatterjee T, Picchioni F, Naskar K. Exploring the influence of electron beam crosslinking in SEBS/TPU and SEBS-g-MA/TPU thermoplastic elastomer blends. Journal of Applied Polymer Science. 2022;139(9):51721. https://doi.org/doi.org/10.1002/app.51721.
[39] Oral E, Godleski Beckos C, Malhi AS, Muratoglu OK. The effects of high dose irradiation on the cross-linking of vitamin E-blended ultrahigh molecular weight polyethylene. Biomaterials. 2008;29(26):3557-3560. https://doi.org/10.1016/j.biomaterials.2008.05.004.
[40] Barboiu V, Avadanei MI. Proposed solution for the Flory–Charlesby equation for crosslinked polymers and application for 1,2-polybutadiene crosslinked with AIBN and aryl diazide. Polymer. 2008;49(21):4687-4694. https://doi.org/10.1016/j.polymer.2008.08.031.
[41] Zhu G, Liang G, Xu Q, Yu Q. Shape-memory effects of radiation crosslinked poly(ϵ-caprolactone). Journal of Applied Polymer Science. 2003;90(6):1589-1595. https://doi.org/10.1002/app.12736.
[42] Olejniczak J, Rosiak J, Charlesby A. Gel Dose Curves for Polymers Undergoing Simultaneous Cross-Linking and Scission. Radiation Physics and Chemistry. 1991;37(3):499-504. https://doi.org/10.1016/1359-0197(91)90026-X.
[43] Hidiroglu M, Aksüt D, Serçe O, Karabulut H, Sen M. Reducing the hydrocarbon gas diffusion and increasing the pressure-impact strength of fuel transfer pipelines for use in the automotive industry using radiation crosslinked polyamide 12. Radiation Physics and Chemistry. 2019;159:118-123. https://doi.org/10.1016/j.radphyschem.2019.02.039.
[44] Bandzierz KS, Reuvekamp LAEM, Przybytniak G, Dierkes WK, Blume A, Bielinski DM. Effect of electron beam irradiation on structure and properties of styrene-butadiene rubber. Radiation Physics and Chemistry. 2018;149:14-25. https://doi.org/10.1016/j.radphyschem.2017.12.011.
[45] Furusawa K, Dobashi T, Morishita S, Oyama M, Hashimoto T, Shinyashiki N, Yagihara S, Nagasawa N. Structural and kinetic modification of aqueous hydroxypropylmethylcellulose (HPMC) induced by electron beam irradiation. Physica a-Statistical Mechanics and Its Applications. 2005;353:9-20. https://doi.org/10.1016/j.physa.2004.12.068.
[46] Rosiak JM. Gel/sol analysis of irradiated polymers. Radiation Physics and Chemistry. 1998;51(1):13-17. https://doi.org/10.1016/S0969-806x(97)00254-5.
[47] Mussatti FG, Macosko CW. Rheology of network forming systems. Polymer Engineering & Science. 1973;13(3):236-240. https://doi.org/https://doi.org/10.1002/pen.760130312.

[48] Reinitz SD, Carlson EM, Levine RAC, Franklin KJ, Van Citters DW. Dynamical mechanical analysis as an assay of cross-link density of orthopaedic ultra high molecular weight polyethylene. Polymer Testing. 2015;45:174-178. https://doi.org/10.1016/j.polymertesting.2015.06.008.
[49] Wang Y, Zhou C, Yi X, Li L, Zhou J, Han X, Gao Y. Research and Evaluation of a New Autogenic Acid System Suitable for Acid Fracturing of a High-Temperature Reservoir. Acs Omega. 2020;XXXX. https://doi.org/10.1021/acsomega.0c00336.
[50] Wang Y, Murcia Valderrama MA, van Putten R-J, Davey CJE, Tietema A, Parsons JR, Wang B, Gruter G-JM. Biodegradation and Non-Enzymatic Hydrolysis of Poly(Lactic-co-Glycolic Acid) (PLGA12/88 and PLGA6/94). Polymers2022.
[51] Villarreal ME, Iturriaga LB. Viscoelastic properties of amaranth starch gels and pastes. Creep compliance modeling with Maxwell model. 2016;68(11-12):1073-1083. https://doi.org/10.1002/star.201600065.
[52] Avrami M. Kinetics of Phase Change. II Transformation-Time Relations for Random Distribution of Nuclei. The Journal of Chemical Physics. 1940;8(2):212-224. https://doi.org/10.1063/1.1750631.
[53] Yang JJ, Pan PJ, Dong T, Inoue Y. Crystallization kinetics and crystalline structure of biodegradable Poly(ethylene adipate). Polymer. 2010;51(3):807-815. https://doi.org/10.1016/j.polymer.2009.11.065.
[54] Svoboda P, Trivedi K, Stoklasa K, Svobodova D, Ougizawa T. Study of crystallization behaviour of electron beam irradiated polypropylene and high-density polyethylene. Royal Society Open Science. 2021;8(3):23. https://doi.org/10.1098/rsos.202250.
[55] Zhao LF, Tian XJ, Liu X, He HF, Zhang J, Zhang RL. Miscibility and Isothermal Crystallization Behavior of Poly (Butylene Succinate-co-Adipate) (PBSA)/Poly (Trimethylene Carbonate) (PTMC) Blends. Journal of Macromolecular Science Part B-Physics. 2016;55(6):591-604. https://doi.org/10.1080/00222348.2016.1179163.
[56] Wang YM, Bhattacharya M, Mano JF. Thermal analysis of the multiple melting behavior of poly(butylene succinate-

-adipate). Journal of Polymer Science Part B-Polymer Physics. 2005;43(21):3077-3082. https://doi.org/10.1002/polb.20589.
[57] Hoffman JD, Frolen LJ, Ross GS, Lauritzen JI. On the growth rate of spherulites and axialites from the melt in polyethylene fractions: regime I and regime II crystallization. Journal of Research of the National Bureau of Standards Section A, Physics and Chemistry. 1975;79(6):671-699. https://doi.org/10.6028/jres.079A.026.
[58] Si PF, Luo FL. Hydrogen bonding interaction and crystallization behavior of poly (butylene succinate-co-butylene adipate)/thiodiphenol complexes. Polymers for Advanced Technologies. 2016;27(11):1413-1421. https://doi.org/10.1002/pat.3809.
[59] Qiu ST, Qiu ZB. Crystallization kinetics and morphology of poly(ethylene suberate). Journal of Applied Polymer Science. 2016;133(12). https://doi.org/10.1002/app.43086.
[60] Yamada K, Hikosaka M, Toda A, Yamazaki S, Tagashira K. Equilibrium melting temperature of isotactic polypropylene with high tacticity: 1. Determination by differential scanning calorimetry. Macromolecules. 2003;36(13):4790-4801. https://doi.org/10.1021/ma021206i.
[61] Fang H, Wu FJ. Nonisothermal Crystallization Kinetics of Poly(butylene terephthalate)/Multiwalled Carbon Nanotubes Nanocomposites Prepared by Polymerization. Journal of Applied Polymer Science. 2014;131(19). https://doi.org/10.1002/App.40849.
[62] Svoboda P, Dvorackova M, Svobodova D. Influence of biodegradation on crystallization of poly (butylene adipate-co-terephthalate). Polymers for Advanced Technologies. 2019;30(3):552-562. https://doi.org/10.1002/pat.4491.

[63] Bandyopadhyay J, Ray SS. Effect of Nanoclay on the Nonisothermal Crystallization of Poly(propylene) and its Blend with Poly[(butylene succinate)-co-adipate]. Molecular Crystals and Liquid Crystals. 2012;556:176-190. https://doi.org/10.1080/15421406.2012.635945.
[64] Chen C, Fei B, Peng SW, Zhuang YG, Dong LS, Feng ZL. Nonisothermal crystallization and melting behavior of poly(3-hydroxybutyrate) and maleated poly(3-hydroxybutyrate). European Polymer Journal. 2002;38(8):1663-1670. https://doi.org/10.1016/S0014-3057(02)00046-0.
[65] Fang H, Wu FJ. Nonisothermal Crystallization Kinetics of Poly(butylene terephthalate)/Multiwalled Carbon Nanotubes Nanocomposites Prepared by

Polymerization. Journal of Applied Polymer Science. 2014;131(19). https://doi.org/10.1002/App.40849.
[66] Jiang G, Wang HT, Yu L, Li HL. Improving crystallization properties of PBSA by blending PBS as a polymeric nucleating agent to prepare high-performance PPC/PBSA/AX8900 blown films. Polymer Engineering and Science. 2022;62(4):1166-1177. https://doi.org/10.1002/pen.25915.
[67] Xu G, Shi WF, Hu P, Mo SP. Crystallization kinetics of polypropylene with hyperbranched polyurethane acrylate being used as a toughening agent. European Polymer Journal. 2005;41(8):1828-1837. https://doi.org/10.1016/j.eurpolymj.2005.02.037.
[68] Huang JW, Wen YL, Kang CC, Tseng WJ, Yeh MY. Nonisothermal crystallization of high density polyethylene and nanoscale calcium carbonate composites. Polymer Engineering and Science. 2008;48(7):1268-1278. https://doi.org/10.1002/pen.21087.
[69] Huang JW, Hung YC, Wen YL, Kang CC, Yeh MY. Polylactide/Nano- and Micro-Scale Silica Composite Films. II. Melting Behavior and Cold Crystallization. Journal of Applied Polymer Science. 2009;112(5):3149-3156. https://doi.org/10.1002/app.29699.
[70] Papageorgiou DG, Papageorgiou GZ, Bikiaris DN, Chrissafis K. Crystallization and melting of propylene-ethylene random copolymers. Homogeneous nucleation and β-nucleating agents. European Polymer Journal. 2013;49(6):1577-1590. https://doi.org/10.1016/j.eurpolymj.2013.02.002.
[71] Wellen RMR, Canedo EL. On the Kissinger equation and the estimate of activation energies for non-isothermal cold crystallization of PET. Polymer Testing. 2014;40:33-38. https://doi.org/10.1016/j.polymertesting.2014.08.008.
[72] Shao YT, Wu CG, Cheng SY, Zhou F, Yan HB. Effects of toughening propylene/ethylene graft copolymer on the crystallization behavior and mechanical properties of polypropylene random-copolymerized with a small amount of ethylene. Polymer Testing. 2015;41:252-263. https://doi.org/10.1016/j.polymertesting.2014.12.008.
[73] Kratochvíl J, Kelnar I. A simple method of evaluating non-isothermal crystallization kinetics in multicomponent polymer systems. Polymer Testing. 2015;47:79-86. https://doi.org/10.1016/j.polymertesting.2015.07.010.

LIST OF FIGURES

LIST OF TABLES

LIST OF ABBREVITATIONS AND SYMBOLS

DMA	Dynamic mechanical analyzer
DSC	Differential scanning calorimetry
EB	Electron beam
EVA	Ethylene-vinyl acetate
G'	Storage modulus
G''	Loss modulus
GPC	Gel permeation chromatography
kGy	Kilogray (unit of absorbed radiation dose)
MFI	Melt flow index
MWD	Molecular weight distribution
N/A	Not applicable
PBS	Poly(butylene succinate)/phosphate-buffered saline
PBSA	Poly(Butylene Succinate-co-Adipate)
PDI	Polydispersity index
PLGA	Poly(Lactic-co-Glycolic Acid)
POM	Polarized optical microscopy
SEC	Size exclusion chromatography
T_g	Glass transition temperature
T_m	Melting temperature
THF	Tetrahydrofuran
$\tan\delta$	Damping factor
VA	Vinyl acetate
WAXD	Wide-angle X-ray diffraction
X	Degree of crystallinity
η^*	Complex viscosity

APPENDIX A

Table A1. Analytical methods used for EVA copolymers

Method	Description
Compression molding (CM)	Preparation of 1 mm thick EVA sheets by ASTM D4703; molded at 150 °C and 10 MPa. Rapid cooling under pressure ensures uniform thickness.
Electron beam irradiation (EB)	Cross-linking via 10 MeV Rhodotron accelerator in air (60–180 kGy); samples sealed between PET sheets; temp < 50 °C.
Dynamic mechanical analysis (DMA) Creep, Stress-Strain, Frequency Sweep	Mechanical testing at 25 °C and 150 °C in shear mode; viscoelastic parameters evaluated using four- and six-parameter models.
Differential scanning calorimetry (DSC)	Thermal analysis to determine crystallinity via heat of fusion; three samples averaged under nitrogen atmosphere.
Wide angle X-ray diffraction (WAXD)	Structural characterization using X-ray diffraction; crystallinity from integrated peak intensities.
Gel content	Solvent extraction in xylene (ASTM D2765-01); insoluble fraction quantified to assess cross-linking.
Size exclusion chromatography (SEC)	Molecular weight analysis using high-temp SEC with TCB as solvent; detection via RI; calibrated with PE standards.

APPENDIX B

Table B1. Analytical methods used for PBSA copolymers

Method	Description
Compression molding (CM)	Test sheets (0.2 mm) prepared by ASTM D4703 at 120 °C and 10 MPa; quenched under pressure.
Hydrolysis at elevated temperature	Samples hydrolyzed in phosphate buffer (pH 7.2) at 37 °C, 58 °C and 70 °C up to 64 days; monitored via DOC and gravimetric mass loss.
Gel permeation chromatography (GPC)	Absolute molar mass determination using RI and VIS detectors; THF solvent; dual detection provides insight into macromolecular architecture.
Differential scanning calorimetry (DSC)	Analysis of isothermal and non-isothermal crystallization; crystallinity and kinetic parameters from multiple temperature programs.
Polarized optical microscopy (POM)	Spherulitic growth observed using polarized optical microscopy and hot stage under controlled cooling.
Wide angle X-ray diffraction (WAXD)	Crystalline structure evaluation using Cu Kα radiation; crystallinity calculated from intensity ratios.

APPENDIX C

Calculation of Charlesby–Pinner parameters for EVA 206

6 wt % of vinyl acetate, M_n = 39000 g/mol

ethylene $= -CH_2 - CH_2-, M_{ET} = 2 \cdot C + 4 \cdot H = 2 \cdot 12.011 + 4 \cdot 1.008$
$= 28.054\ g/mol$

vinyl acetate $= C_4H_6O_2, M_{VA} = 4 \cdot C + 6 \cdot H\ + 2 \cdot O$
$= 4 \cdot 12.011 + 6 \cdot 1.008 + 2 \cdot 16 = 86.092\ g/mol$

$$\text{wt. fraction of vinyl acetate } w_{VA} = \frac{6}{100} = 0.06$$

$$\text{wt. fraction of ethylene } w_{ET} = 1 - w_{VA} = 1 - 0.06 = 0.94$$

$$\text{Molar fraction of vinyl acetate } = x_{VA}$$

$$x_{VA} = \frac{\frac{w_{VA}}{M_{VA}}}{\frac{w_{VA}}{M_{VA}} + \frac{w_{ET}}{M_{ET}}} = \frac{\frac{0.06}{86.092}}{\frac{0.06}{86.092} + \frac{0.94}{28.054}} = 0.02038$$

$$\text{Molar fraction of ethylene } = x_{ET} = 1 - x_{VA} = 1 - 0{,}020378 = 0.97962$$

Average molecular weight of repeating unit:

$$M_{ET-VA} = x_{ET}M_{ET} + x_{VA}M_{VA} = 0.97962 \cdot 28.054 + 0.02038 \cdot 86.092$$
$$= 29.2368\ g/mol$$

$$\text{Polymerization degree } = P_n = \frac{M_{nVA}}{M_{ET-VA}} = \frac{39000}{29.2368} = 1334$$

Charlesby–Pinner equation:

$$s + \sqrt{s} = \frac{p_0}{q_0} + \frac{1}{q_0 P_n D}$$

$$\text{In plot } s + \sqrt{s}\ vs. \frac{1}{D} : intercept = \frac{p_0}{q_0}, slope\ \frac{1}{q_0 P_n}$$

In case of EVA 206: intercept = 0.3246, slope = 55.072

$$\text{then } \frac{p_0}{q_0} = 0.3246 \text{ and } \frac{1}{q_0 P_n} = 55.072$$

$$q_0 = \frac{1}{slope \cdot P_n} = \frac{1}{55.072 \cdot 1334} = 0.00001361$$

$$\text{then } p_0 = q_0 \cdot intercept = q_0 \cdot \frac{p_0}{q_0} = 0.00001361 \cdot 0.3246 = 0.000004418$$

Calculation of G parameters according to Charlesby-Pinner equation (see Table S2):

$$s + \sqrt{s} = \frac{G(S)}{2G(X)} + \frac{4.82 \times 10^6}{G(X) M_n D}$$

$$\text{then } \frac{G(S)}{2G(X)} = \frac{p_0}{q_0}$$

$$\frac{G(X)}{G(S)} = \frac{1}{2\frac{p_0}{q_0}} = \frac{1}{2 \cdot 0.3246} = 1.5404$$

$$\text{slope} = \frac{4.82 \times 10^6}{G(X)M_n}$$

$$G(X) = \frac{4.82 \times 10^6}{slope \cdot M_n} = \frac{4.82 \times 10^6}{55.072 \cdot 39000} = 2.2441$$

$$\text{Intercept} = \frac{G(S)}{2G(X)}$$

$$G(S) = 2 \cdot G(X) \cdot intercept = 2 \cdot 2.2441 \cdot 0.3246 = 1.4569$$

Calculation of Charlesby–Pinner parameters for EVA 212

12 wt % of vinyl acetate, M_n = 34000 g/mol

ethylene $= -CH_2 - CH_2-, M_{ET} = 2 \cdot C + 4 \cdot H = 2 \cdot 12.011 + 4 \cdot 1.008 = 28.054\ g/mol$

Vinyl acetate $= C_4H_6O_2, M_{VA} = 4 \cdot C + 6 \cdot H + 2 \cdot O = 4 \cdot 12.011 + 6 \cdot 1.008 + 2 \cdot 16 = 86.092\ g/mol$

$$\text{wt. fraction of vinyl acetate } w_{VA} = \frac{12}{100} = 0.12$$

$$\text{wt. fraction of ethylene } w_{ET} = 1 - w_{VA} = 1 - 0{,}12 = 0.88$$

$$\text{Molar fraction of vinyl acetate} = x_{VA}$$

$$x_{VA} = \frac{\frac{w_{VA}}{M_{VA}}}{\frac{w_{VA}}{M_{VA}} + \frac{w_{ET}}{M_{ET}}} = \frac{\frac{0.12}{86.092}}{\frac{0.12}{86.092} + \frac{0.88}{28.054}} = 0.04255.$$

Molar fraction of ethylene $= x_{ET} = 1 - x_{VA} = 1 - 0.04255 = 0.95745$

Average molecular weight of repeating unit:

$$M_{ET-VA} = x_{ET}M_{ET} + x_{VA}M_{VA} = 0.95745 \cdot 28.054 + 0.04255 \cdot 86.092 = 30.5235\ g/mol$$

$$\text{Polymerization degree} = P_n = \frac{M_{nVA}}{M_{ET-VA}} = \frac{34000}{30.5235} = 1114$$

Charlesby–Pinner equation:

$$s + \sqrt{s} = \frac{p_0}{q_0} + \frac{1}{q_0 P_n D}$$

$$\text{In plot } s + \sqrt{s}\ vs. \frac{1}{D}: intercept = \frac{p_0}{q_0}, slope\ \frac{1}{q_0 P_n}$$

In case of EVA 212: intercept = 0.2163, slope =58.972

$$\text{then } \frac{p_0}{q_0} = 0.2163\ and\ \frac{1}{q_0 P_n} = 58.972$$

$$q_0 = \frac{1}{slope \cdot P_n} = \frac{1}{58.972 \cdot 1114} = 0.00001522$$

$$\text{then } p_0 = q_0 \cdot intercept = q_0 \cdot \frac{p_0}{q_0} = 0.00001522 \cdot 0.2163 = 0.000003292.$$

Calculation of G parameters according to Charlesby-Pinner equation (see Table B1):

$$s + \sqrt{s} = \frac{G(S)}{2G(X)} + \frac{4.82 \times 10^6}{G(X)M_n D}$$

$$\text{then } \frac{G(S)}{2G(X)} = \frac{p_0}{q_0}$$

$$\frac{G(X)}{G(S)} = \frac{1}{2\frac{p_0}{q_0}} = \frac{1}{2 \cdot 0.2163} = 2.3116$$

$$\text{slope } = \frac{4.82 \times 10^6}{G(X)M_n}$$

$$G(X) = \frac{4.82 \times 10^6}{58.972 \cdot 34000} = 2.4039$$

$$\text{Intercept } = \frac{G(S)}{2G(X)}$$

$$G(S) = 2 \cdot G(X) \cdot intercept = 2 \cdot 2.4039 \cdot 0.2163 = 1.0399$$

Table C1. Calculated Charlesby–Pinner parameters.

Material	**wt% of VA**	**wt.fraction of VA**	**wt.fraction of ET**	**Molar fraction of VA**
EVA206	6	0.06	0.94	0.0204
EVA212	12	0.12	0.88	0.0425
Material	**Molar fraction of ET**	**$M_{ET\text{-}VA}$**	**M_n**	**P_n**
EVA206	0.9796	29.2366	39000	1333.95
EVA212	0.9575	30.5232	34000	1113.91
Material	**Slope**	**p_0/q_0**	**q_0**	**p_0**
EVA206	55.0716	0.3246	0.00001361	0.000004418
EVA212	58.9716	0.2163	0.00001522	0.000003293
Material	**G(X)/G(S)**	**G(X)**	**G(S)**	
EVA206	1.5405	2.2442	1.4568	
EVA212	2.3116	2.404	1.0399	

LIST OF PUBLICATIONS

Articles published in journals indexed on Web of Science

[1] Svarcova A, Svoboda P. Enhanced Mechanical Properties of Irradiated Ethylene-Vinyl Acetate Copolymer. Processes. 2025;13(5):31. https://doi.org/10.3390/pr13051562.

[2] Svarcova A, Svoboda P. Dynamic Mechanical and Charlesby-Pinner Analyses of Radiation Cross-Linked Ethylene-Vinyl Acetate Copolymer (EVA). Molecules. 2025;30(7). https://doi.org/10.3390/molecules30071485.

[3] Svarcova A, Dvorackova M, Svoboda P. Influence of Hydrolysis on Non-Isothermal Crystallization of Poly(Butylene Succinate-Co-Adipate) (PBSA). Molecules. 2025;30(11):25. https://doi.org/10.3390/molecules30112252.

[4] Svarcova, A.; Svoboda, P. Hoffman–Lauritzen Analysis of Crystallization of Hydrolyzed Poly(Butylene Succinate-Co-Adipate). Crystals **2025**, 15, 645. https://doi.org/10.3390/cryst15070645.

CURICULUM VITAE

Name:	Anna ŠVARCOVÁ
Date of birth:	22nd May 1995
Place of birth:	Hradec Králové
Nationality:	Czech
Permanent address:	Jezernice 136, 751 31 Czech Republic
Affiliation:	Department of Polymer Engineering, Faculty of Technology, Tomas Bata University in Zlin, Vavreckova 5669, 76001 Zlin, Czech Republic
E-mail:	a_svarcova@utb.cz

Education:	2020 – to date Doctoral degree Faculty of Technology Tomas Bata University in Zlin (Czech Republic) **Technology of Macromolecular Substances**
Education:	2018 – 2020 Master's degree Faculty of Technology Tomas Bata University in Zlin (Czech Republic) **Polymer Engineering**
Education:	2015 – 2018 Bachelor's degree Faculty of Technology Tomas Bata University in Zlin (Czech Republic) **Polymeric Materials and Technology**
Education stays:	**November-December 2024** Czestochowa University of Technology, Department of Technology and Automation, Aleja Armii Krajowej 21, 42-200 / Czestochowa, Poland
Projects:	**Internal funding** • IGA/FT/2024/008 - Study of Polymeric Systems – Preparation and Evaluation of Properties

Anna Švarcová

Influence of Irradiation and Hydrolysis on Mechanical Properties and Crystallization in Selected Copolymers

Vliv ozařování a hydrolýzy na mechanické vlastnosti a krystalizaci u vybraných kopolymerů

Doctoral Thesis Summary

Published by: Tomas Bata University in Zlín

nám. T. G. Masaryka 5555, 760 01 Zlín.

Edition: Doctoral Thesis Summary

Typesetting by: Anna Švarcová

The publication has not undergone any proofreading or editorial revision.

Year of publication: 2025

First Edition

ISBN 978-80-7678-388-1